# Storage, evolution, and mixing in basaltic eruptions from around the Okataina Volcanic Centre, Taupō Volcanic Zone, Aotearoa New Zealand

Ery C. Hughes: Te Pū Ao | GNS Science (e.hughes@gns.cri.nz)
Sally Law:
School of GeoSciences, University of Edinburgh (Sally.Law@ed.ac.uk)
Geoff Kilgour: Te Pū Ao | GNS Science (g.kilgour@gns.cri.z)
Jon D. Blundy: University of Oxford (jonathan.blundy@earth.ox.ac.uk)
Heidy M. Mader: University of Bristol(h.m.mader@bristol.ac.uk)

This paper is a revised version of a non-peer review pre-print submitted to EarthArXiv, which has been submitted to the Journal of Volcanology and Geothermal Research special issue on the Okataina Volcanic Centre for peer review.

Twitter handles: @eryhughes, @sallylaw, @NZvolcanologist

# Storage, evolution, and mixing in basaltic eruptions from around the Okataina Volcanic Centre, Taupō Volcanic Zone, Aotearoa New Zealand

Ery C. Hughes[1,2,3*], Sally Law[4], Geoff Kilgour[5], Jon D. Blundy[6], and Heidy M. Mader[1]

1 School of Earth Sciences, University of Bristol, Wills Memorial Building, Queens Road, Bristol BS8 1RJ, UK

2 Division of Geological and Planetary Sciences, California Institute of Technology, Arms Laboratory, Pasadena, CA 91125, USA

3 Volcanology Team, National Isotope Centre/Avalon, Te Pū Ao | GNS Science, Lower Hutt, Aotearoa New Zealand

4 School of GeoSciences, University of Edinburgh, King's Buildings, Edinburgh EH9 3FE, UK

5 Volcanology Team, Wairakei Research Centre, Te Pū Ao | GNS Science, Taupō, Aotearoa New Zealand

6 Department of Earth Sciences, University of Oxford, South Parks Road, Oxford OX1 3AN, UK

*Corresponding author. Email: e.hughes@gns.cri.nz

## Abstract

The Okataina Volcanic Centre (OVC) is the most recently active caldera system in the Taupō Volcanic Zone, Aotearoa New Zealand. Although best known for its high rates of explosive rhyolitic volcanism, there are several examples of basaltic to basaltic-andesite contributions to OVC eruptions. These range from minor involvement of basalt in rhyolitic eruptions to the exclusively basaltic 1886 C.E. plinian eruption of Tarawera. To explore the basaltic component supplying this dominantly rhyolitic area, we analyse the textures and compositions (minerals and melt inclusions) of four basaltic eruptions from within and around the OVC that have similar whole rock chemistry, namely: Terrace Rd, Rotomakariri, Rotokawau, and Tarawera. Data from these basaltic deposits provide constraints on the conditions of magma evolution and ascent in the crust prior to eruption, revealing that eruptions sample multiple distinct reservoirs during ascent to the surface. The most abundant basaltic component is generated by cooling-induced crystallisation of a common, oxidised, volatile-rich basaltic melt at various depths within the crust that mixes upon ascent. Despite similar bulk compositions, these four eruptions are texturally distinct from each other as a result of their wide variation in eruption style.

**Keywords:** geochemistry, Tarawera, Terrace Rd, Rotomakariri, Rotokawau, melt inclusions

## 1 Introduction

Volcanic arcs are characterised by complicated sub-surface architectures that convert basaltic mantle-derived melt into a wide variety of more evolved arc magma compositions (e.g., reviews by Ducea et al., 2015; Grove et al., 2012). Compositional variability can be derived from variations in the primary composition of the mantle melt input, extents of crustal assimilation, type of petrological processes occurring (e.g., crystallisation, degassing, mixing), and the conditions of magma stagnation (pressure, temperature). Static models that account for the evolution of melt composition in the crust are achieved through variations in temperature

(e.g., Annen et al., 2006), whereas dynamic models drive compositional variation by reactive melt percolation (e.g., Jackson et al., 2018); both mechanisms have been used to explain the compositional variability of arc magmas. Reconciling these models requires observations and analysis of volcanic rocks or exhumed crustal sections, which provide snapshots and time-integrated histories, respectively, of magmatic systems.

Both crustal and erupted materials at arcs are dominated by evolved magma compositions (i.e., andesites to rhyolites) despite the large inputs of basaltic melt required for their formation. Most basalts never reach the surface due to relatively high magma density compared to the surrounding crust. Furthermore, these intrusions cool in the crust and either solidify to gabbroic plutons or generate more evolved magmas that separate and ascend to then erupt or cool to form felsic plutons. Any basaltic magmas that do reach the surface will have traversed this complicated crustal region yet unravelling this cryptic differentiation history is not trivial and inevitably requires high resolution, *in situ* mineral analysis. Here, we utilise microanalytical geochemical methods to collect data on crystals and their melt inclusions to explore the paths taken by basaltic magmas beneath a dominantly rhyolitic caldera. We constrain how and where basaltic magmas are stored within the crust, and what petrological processes affect them. This is important for assessing the current state of magma reservoirs in the crust in the context of geophysical surveys and predicting potential precursory signals before future eruptions.

The Okataina Volcanic Centre (OVC) is one of two currently active caldera systems in the Taupō Volcanic Zone, Aotearoa New Zealand (Taupō Volcanic Centre, TVC, is the other). From several studies of the rhyolites, the sub-surface architecture below the OVC is known to comprise discrete rhyolitic melt-mush pockets that erupt compositionally distinct magmas within single eruptions (e.g., Cole et al., 2014; Sas et al., 2021; Shane et al., 2008a, 2007; Smith et al., 2004; Storm et al., 2011). Basaltic magmas are key to generating the more evolved magma compositions in the OVC, but little is known about their evolution. Heat and volatiles are assumed to be transferred between basalts and rhyolites to trigger rhyolitic eruptions (e.g., Leonard et al. 2002; Shane et al. 2007, 2008; Smith et al. 2010), but the initial volatile contents of the basalts are largely unconstrained. Abundant evidence for basaltic-rhyolitic magma interaction also enables investigation of how magma mixing is related to basaltic eruption style (e.g., Leonard et al., 2002; Shane et al., 2005). In this study we combine textural observations with mineral and melt inclusion chemistries to constrain the magmatic compositions (including volatiles), conditions, and processes occurring during crustal storage and ascent of basaltic magmas around the OVC.

## 2 Regional setting

The Taupō Volcanic Zone (TVZ) is the most frequently active and productive silicic system on Earth (Wilson et al., 2009). Oblique subduction of the Pacific plate under continental Zealandia leads to the clockwise rotation of the eastern portion of the North Island, resulting in extension in the TVZ, crustal thinning, and basalt underplating (Houghton et al., 1995; Mortimer et al., 2017; Wilson et al., 1995). High rates of underplating drive the generation of voluminous silicic magma and, together with the relatively thin and faulted crust, enhance magma production and the rate of eruptions (e.g., Cole et al., 2014; Price et al., 2005). Extensive crustal contamination influences the isotopic composition of TVZ basalts and rhyolites (e.g., Gamble et al., 1993; Graham et al., 1995; Sas et al., 2021; Waight et al., 2017).

Basalts are volumetrically minor at the surface compared to andesites/dacites (ten times greater in volume) and rhyolites (100 to 1000 times greater in volume) (Wilson et al., 1995). TVZ basalts are classified as high-alumina and are generated by a combination of rift-induced

decompression melting and fluid-induced flux melting (Hiess et al., 2007; Law et al., 2021). Active calderas have high inputs of basalt from the mantle wedge, which is caused by fluid-fluxed melting of relatively fertile mantle (Barker et al., 2020; Zellmer et al., 2020). The mantle source under these calderas is lherzolitic, as the sub-continental lithospheric mantle has been removed by rifting and crustal thinning, shifting volcanism to rhyolitic rather than andesitic (Law et al., 2021). Regions without active calderas have lower inputs of basalt due to either a subdued influence from fluid-fluxing or a more depleted mantle source, plausibly caused by prior mantle melt extraction associated with formation of older calderas (Barker et al., 2020; Zellmer et al., 2020). Basaltic eruptions throughout the TVZ are often associated with faults and commonly erupt in association with rhyolitic magmas (Cole, 1970a; Hiess et al., 2007; Nairn and Cole, 1981). Basaltic volcanism exhibits a wide range of eruption style, both within and between individual eruptions and volcanic centres, and shallow conduit processes (including interaction with external, non-magmatic water) are thought to play a major role in determining eruption style (e.g., Carey et al., 2007; Houghton and Hackett, 1984).

The currently active OVC is overwhelmingly rhyolitic, but a diverse range of styles and intensities of basaltic explosive activity is also present within and outside the caldera (Cole et al., 2014; Nairn, 2002) (Figure 1a). Since ~55 ka there have been at least six basaltic eruptions in this region, ranging from phreatomagmatic to magmatic and strombolian to plinian in intensity (Table 1 and Figure 1) in addition to two examples of mafic enclaves and blebs in exclusively rhyolitic eruptions (Cole et al., 2014; Nairn, 2002). Basaltic plinian eruptions are rare in the geological record, and Tarawera is the one of the most recent (Cole, 1970a; Nairn, 1979; Rowe et al., 2021; Thomas, 1888; Walker et al., 1984).

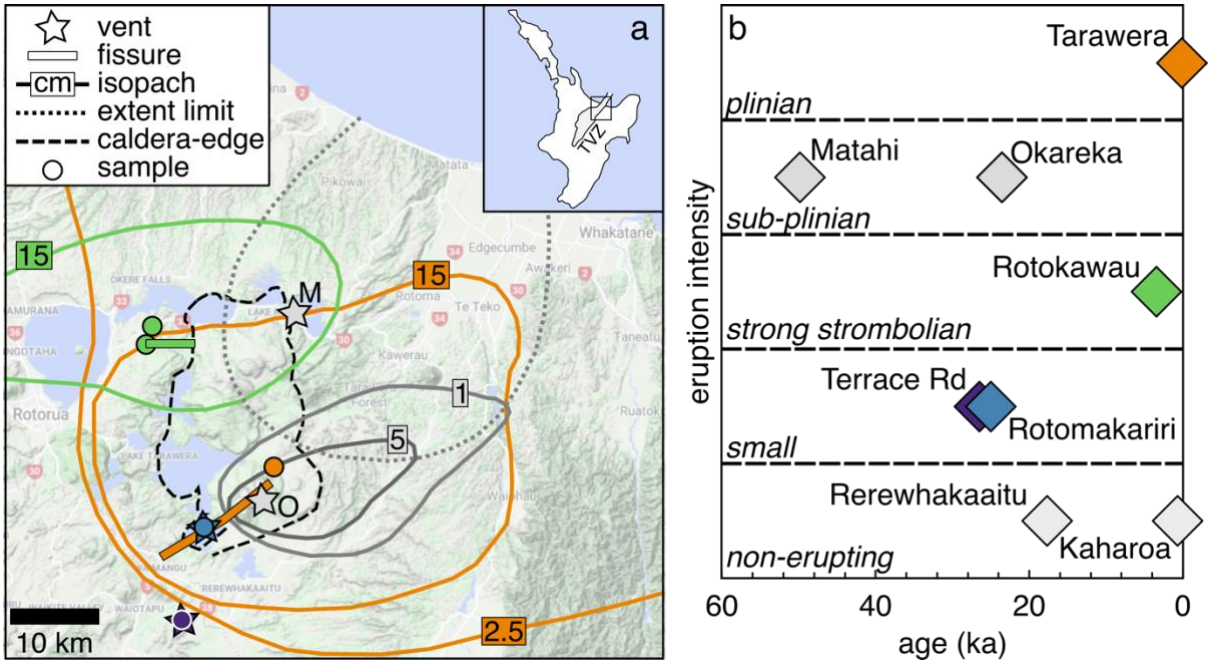


*Figure 1* **(a)** Map of the region surrounding the Okataina Volcanic Centre (OVC), showing the caldera boundary (black dashed curve); location of eruptive vents and fissures (coloured stars or lines; Beanland, 1989; Burt et al., 1998; Darragh et al., 2006; Nairn, 2002, 1992); deposit thickness isopleths or extent limit (solid or dashed cruves; Beanland, 1989; Darragh et al., 2006; Nairn, 1992; Pullar and Nairn, 1972); and sample locations for this study for the basaltic eruptions (circles). Colour indicates eruption as shown in (b) – eruptions analysed in this study are in colour and other basalts from around the OVC are shown in grey. Inset shows the location of the main map and the Taupō Volcanic Zone (TVZ, shaded area) in the North Island of Aotearoa New Zealand. M = Matahi, where the dotted-grey line is the extent limit; and O = Okareka, where the solid-grey lines are the 1 and 5 cm isopachs. **(b)** Qualitative eruption intensity against age (Buck et al., 2003; Hogg et al., 2003; Hopkins et al., 2021; Nairn, 2002; Newnham et al., 2003; Peti et al., 2021) for OVC basaltic magmas – Rerewhakaaitu and Kaharoa do not appear in (a) because they only occur as basaltic enclaves and blebs within a rhyolitic eruption.

*Table 1* Basalts from around the Okataina Volcanic Centre (OVC) since the last caldera-forming eruption.

| Eruption | Age (ka) | Description | DRE volume ($km^3$) [Column height (km)] |
|---|---|---|---|
| Tarawera* | 1886 C.E. | Phreatomagmatic to magmatic, strombolian to plinian fissure[1–3] | 0.25–0.48[4] [~28][3] |
| Kaharoa | 0.6[5–6] | Enclaves in rhyolitic eruption[7–9] | >0.01[9] |
| Rotokawau* | 3.44 ± 0.07[10] | Phreatomagmatic (surtseyan) and strombolian fissure[10–12] | 0.55[11] [4.5–7][11] |
| Rerewhakaaitu | 17.6[13] | Blebs in rhyolitic eruption[14] | n.d. |
| Okareka | 23.5[15] | Single vent, sub-plinian phase prior to rhyolitic eruption[16–17] | 0.01[16,18] |
| Rotomakariri* | 22–28[10] | Single vent tuff cone[10] | n.d. |
| Terrace Rd* | 25–28, 28 ± 2[10] | Single vent (?), small phreatomagmatic[10] | n.d. |
| Matahi† | ~45–55[19] | Single vent, sub-plinian[20] | <1[21] |

*Notes:* *Eruptions analysed in this study. †The Matahi eruption occurred just prior to the Rotoiti Ignimbrite that was the most recent OVC caldera-forming eruption. Volumes (DRE = dense rock equivalent) for Terrace Rd and Rotomakariri are not determined (n.d.), but are likely small due to their limited occurrence (Nairn, 2002). References: [1]Keam (1988), [2]Nairn and Cole (1981), [3]Walker et al. (1984), [4]Rowe et al. (2021), [5]Hogg et al. (2003), [6]Buck et al. (2003) [7]Leonard et al. (2002), [8]Nairn et al. (2001), [9]Nairn et al. (2004), [10]Nairn (2002), [11]Beanland (1989), [12]Beanland and Houghton (1978), [13]Newnham et al. (2003), [14]Shane et al., (2007), [15]Peti et al. (2021), [16]Darragh et al. (2006), [17]Nairn (1992), [18]Shane et al. (2008a), [19]see discussion in Hopkins et al. (2021), [20]Pullar and Nairn (1972), and [21]Froggatt and Lowe (1990).

Basaltic eruptions around the OVC are fed by dikes. Vents are often aligned along the main NE-SW trending tectonic fabric, predominantly along the Tarawera Linear Vent Zone, but also just outside the caldera boundaries (Nairn, 2002; Figure 1a). Most individual eruptions issued from a single vent, but the Tarawera and Rotokawau eruptions occurred along fissures, displaying a range of style and intensity both spatially and temporally within each eruption (Nairn, 2002). For instance, the Tarawera eruption generated a ~17 km-long fissure, with strombolian to plinian magmatic eruptions in the NE and phreatomagmatic eruptions in the SW where it intersected an active hydrothermal system (Nairn, 1979; Nairn and Cole, 1981; Rowe et al., 2021; Walker et al., 1984). The Tarawera fissure is broadly perpendicular to the TVZ extension direction, in marked contrast to the E-W striking Rotokawau fissure (Beanland, 1989).

Many OVC rhyolitic eruptions are likely triggered by the injection of basaltic magmas (e.g., Leonard et al., 2002; Shane et al., 2008, 2007). Some rhyolitic eruptions were preceded by basaltic eruptions, with either no (e.g., Matahi prior to Rotoiti) or direct (e.g., mixed basaltic-rhyolitic clasts in Okareka) evidence for magma mixing prior to eruption, whereas others (e.g., Rerewhakaaitu and Kaharoa) host basaltic blebs and enclaves (e.g., Burt et al., 1998; Cole, 1973a; Cole et al., 2014; Leonard et al., 2002; Nairn, 1992; Pullar and Nairn, 1972; Schmitz and Smith, 2004; Shane et al., 2007, 2008a). The OVC is passively degassing $CO_2$ and heat today, and inferred basaltic dike intrusion events also occur, as well as evidence for cooling intrusions (e.g., Benson et al., 2021; Hamling et al., 2022; Hughes et al., 2019b; Mazot et al., 2014; Seward et al., 2022; Yang et al., in review).

All basalts (including blebs in rhyolitic eruptions) from around the OVC contain olivine, clinopyroxene, and plagioclase crystals (sometimes in aggregates) within a glassy (e.g., Matahi) to highly microcrystalline groundmass (e.g., Cole, 1970b; Law et al., 2021; Nairn, 2002, 1992; Rowe et al., 2021; Sable et al., 2009; Schmitz and Smith, 2004; Shane et al., 2008a). Additionally, most basalts contain entrained xenocrystic quartz and rhyolitic material (Beanland, 1989; Cole, 1973a; Nairn, 2002; Schmitz and Smith, 2004). Since ~55 ka in the

OVC, hornblende has only been observed in basaltic enclaves in the Kaharoa eruption (Leonard et al., 2002). Clast vesicularity ranges from dense to highly vesicular, even within a single eruption (Beanland, 1989; Nairn, 2002; Shane et al., 2008). Dense clasts are often used as evidence for interaction with external water (e.g., Beanland and Houghton, 1978; Carey et al., 2007).

## 3 Methods

We studied material from the Terrace Rd, Rotomakariri, Rotokawau, and Tarawera eruptions as they cover the full range of eruption styles and sizes (phreatomagmatic to magmatic and strombolian to plinian) observed around the OVC (Figure 1b). Rotomakariri and Tarawera occurred inside the caldera boundary (along one of the main linear vent zones), whereas Terrace Rd and Rotokawau occurred outside (Figure 1a). There are no published melt inclusion data for Terrace Rd, Rotomakariri, and Rotokawau, and only limited published data for Tarawera (Barker et al., 2020; Rowe et al., 2021); melt inclusions have been previously analysed from Okareka and Kaharoa (Barker et al. 2020).

To constrain pre-eruptive magmatic compositions, conditions, and processes, we analysed mineral and melt inclusion chemistry and textures. Scoria 4–8 mm in size were selected to ensure rapid clast cooling and Tarawera samples were collected off the volcano to avoid material that had cooled slowly. This increases the potential for glassy melt inclusions that retain their initial volatile content (Lloyd et al., 2013). Olivine, pyroxene, and plagioclase crystals were hand-picked from gently crushed clasts and either bulk mounted in epoxy or individually mounted and polished to expose a melt inclusion. Only naturally glassy clinopyroxene-hosted melt inclusions were analysed; no rehomogenisation experiments were carried out.

Olivine, pyroxene, and plagioclase were analysed using electron probe micro-analysis (EPMA) wavelength dispersive spectrometry (WDS). Unless otherwise stated, all analyses were taken from crystal cores. Melt inclusions from all eruptions were analysed using EPMA-WDS for major, minor, and volatile (S, Cl, and F) elements and for $H_2O$ using calibrated volatiles-by-difference (Hughes et al., 2019a). A subset of melt inclusions from Tarawera was analysed for $H_2O$ and $CO_2$ using secondary ion mass spectrometry (SIMS) prior to EPMA. To put mineral separate data into context, textural observations on thin sections were made using optical microscopy and scanning electron microscopy (SEM). Some mineral phases (and the groundmass glass for Rotomakariri) in the thin sections were analysed using semi-quantitative (sq) SEM energy dispersive spectroscopy (EDS) (sq-SEM-EDS) and EPMA-WDS to correlate the textures with mineral separates data.

To expand our dataset, we compiled mineral, melt inclusion, and whole rock data from the literature, particularly from basaltic eruptions not analysed in this study (e.g., Matahi, Okareka, Rerewhakaaitu, and Kaharoa). Several thermometers (melt, olivine-melt, clinopyroxene-melt, and clinopyroxene-orthopyroxene; Putirka, 2008), oxybarometers (melt $Fe^{3+}/Fe_T$; Kress and Carmichael, 1991), and barometers (clinopyroxene-melt; Neave and Putirka, 2017, and $H_2O$-$CO_2$ melt concentrations; Ghiorso and Gualda, 2015), as well as rhyolite-MELTS modelling (Ghiorso and Gualda, 2015; Gualda et al., 2012), were applied to mineral, melt inclusion, and whole rock data from this study and the literature. Only mineral-mineral and mineral-melt pairs that correspond to established equilibrium models are presented. Data collection and reporting for melt inclusions broadly follows the guidelines of Rose-Koga et al. (2021). Full analytical and calculation details, as well as all data collected and compiled, are provided in Supplementary Material.

## 4 Textural and chemical characteristics

### *4.1 Vesicles, groundmass, and macrocrysts*

Texturally and chemically, Tarawera, Rotokawau, and Terrace Rd scoria are more similar to each other than to scoria from Rotomakariri. Tarawera, Rotokawau, and Terrace Rd are characterised by vesicles with complex shapes in a highly crypto- to microcrystalline groundmass containing olivine, clinopyroxene, plagioclase, and Fe-Ti oxide microlites (Figure 2a, c, and d). Rotokawau and Tarawera scoria are homogeneously brown-to-black, whereas Terrace Rd is highly variable in colour (black to light-brown), including small domains (<3 mm across) of black and grey material. At Terrace Rd, the mineralogy and texture of the groundmass is very similar in both the brown and black areas; Rotokawau also shows multiple groundmass textures, including flow alignment (Figure 2p). Rotomakariri scoria are homogeneously brown-to-black and have rounded vesicles in a groundmass of glass containing sparse microlites of plagioclase and clinopyroxene (Figure 2b). Further details are in Supplementary Material.

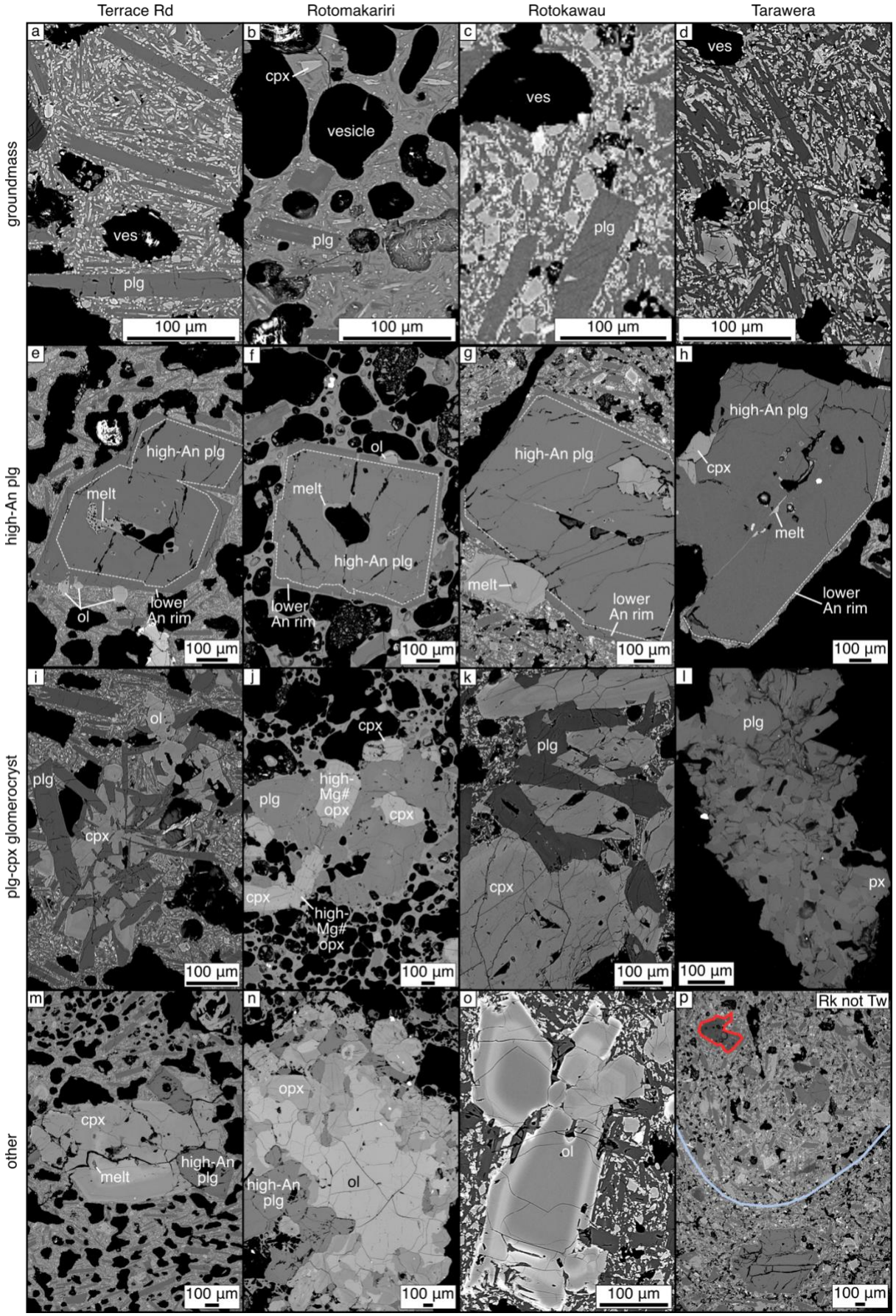


239

240 *Figure 2* Annotated back-scattered electron (BSE) scanning electron microscope (SEM) images of scoria textures.
241 Each column is a separate eruption: Terrace Rd (a, e, i, m), Rotomakariri (b, f, j, n), Rotokawau (c, g, k, o, and

additionally p at the bottom of the far-right column), and Tarawera (d, h, l). Different features are shown by row. **(a–d)** Groundmass textures, where in **(b)** plagioclase is $An_{76}$. **(e–h)** High-An plagioclase ($An_{93–96}$ cores and $An_{76–87}$ rims) forms glomerocrysts with other phases. **(i–m)** Glomerocrysts of plagioclase and pyroxene: **(i)** intergrowths of plagioclase and clinopyroxene, with altered olivine at the edge of the intergrowth; **(j)** plagioclase (core $An_{83}$, rim $An_{79}$), clinopyroxene (Mg# 75–78), and high-Mg# orthopyroxene (Mg# = 71 core, 75 rim); **(k)** clinopyroxene (Mg# 85) and plagioclase ($An_{88}$); **(l)** intergrown plagioclase and pyroxene; **(m)** high-An plagioclase and olivine ($Fo_{76}$) attached to a clinopyroxene (Mg# = 65 core, 80 middle, 73 rim). **(n–p)** Other textures: **(n)** glomerocryst: centre is a partially resorbed olivine ($Fo_{83}$), with overgrowths of high-Mg# orthopyroxene (Mg# 76), high-An plagioclase ($An_{92}$ core, $An_{85}$ rim), and some clinopyroxene around the edge of the olivine grain; **(o)** olivine macrocryst (dark portions $Fo_{80}$, bright band $Fo_{75}$); and **(p)** alignment of plagioclase from basalt-basalt mixing (blue line) and region of evolved material is outlined in red. *Abbreviations:* ves = vesicle, ol = olivine, plg = plagioclase, cpx = clinopyroxene, opx = orthopyroxene, and px = pyroxene.

Terrace Rd, Rotokawau, and Rotomakariri contain abundant macrocrysts, mostly as glomerocrysts (Figure 2i–n), whereas Tarawera is almost macrocryst- and glomerocryst-free (see also Law et al., 2021). All eruptions have a similar mineralogy of olivine, plagioclase, and clinopyroxene, with Rotomakariri additionally containing abundant orthopyroxene. Alkali feldspars and quartz were found in all eruptions. Olivine composition varies between eruptions, with a narrow range in forsterite (Fo) content at Terrace Rd ($Fo_{76–79}$) and Tarawera ($Fo_{79–85}$) and a wide range at Rotomakariri ($Fo_{71–82}$) and Rotokawau ($Fo_{73–82}$) (Figure 3a–e). Groundmass olivine from Tarawera analysed by Rowe et al. (2021) has similar Fo to the macrocrysts (Figure 3a). Clinopyroxene composition is similar across all eruptions, including groundmass clinopyroxene from Tarawera reported by Rowe et al. (2021), with Mg# 69–87 (Figure 3f–k). Orthopyroxene from Rotomakariri is bimodal in composition (Figure 3h). High-Mg# orthopyroxene (83–87) is found as macrocrysts in Rotomakariri (and rarely Rotokawau and Tarawera) and sometimes as inclusions in clinopyroxene at Terrace Rd and Rotokawau. Low-Mg# orthopyroxene (67–83), sometimes with inclusions of apatite, occurs in all eruptions. Plagioclase displays a wide range of anorthite content (Figure 3k–o). Some "high-An" plagioclase grains have very calcic ($>An_{90}$) cores with coarse sieving and normal zoning to a thin, unsieved, less calcic rim (Figure 2e–h). At Terrace Rd, $>An_{90}$ was not measured via EPMA on picked grains but was observed in SEM images (e.g., Figure 2e). Many plagioclase crystals have lower An (55–90), are mostly unzoned, and occur as both macrocrysts and inclusions in clinopyroxene at Terrace Rd, in low-Mg# orthopyroxene at Rotokawau, and in both clinopyroxene and orthopyroxene at Rotomakariri. This plagioclase composition is similar to rims on the highly calcic plagioclase and plagioclase microlites in the Tarawera groundmass (Rowe et al., 2021). For plagioclase with $>An_{55}$, FeO content is high (>0.4 wt%) and decreases with increasing An (see Figure S6 in Supplementary Material). There are some "low-An", texturally variable plagioclases with $An_{<55}$ and FeO <0.4 wt%. Unlike mineral compositions, which are similar across different eruptions, glomerocrysts are unique to individual eruptions. More detailed descriptions of both the minerals and glomerocrysts are provided in Supplementary Material.

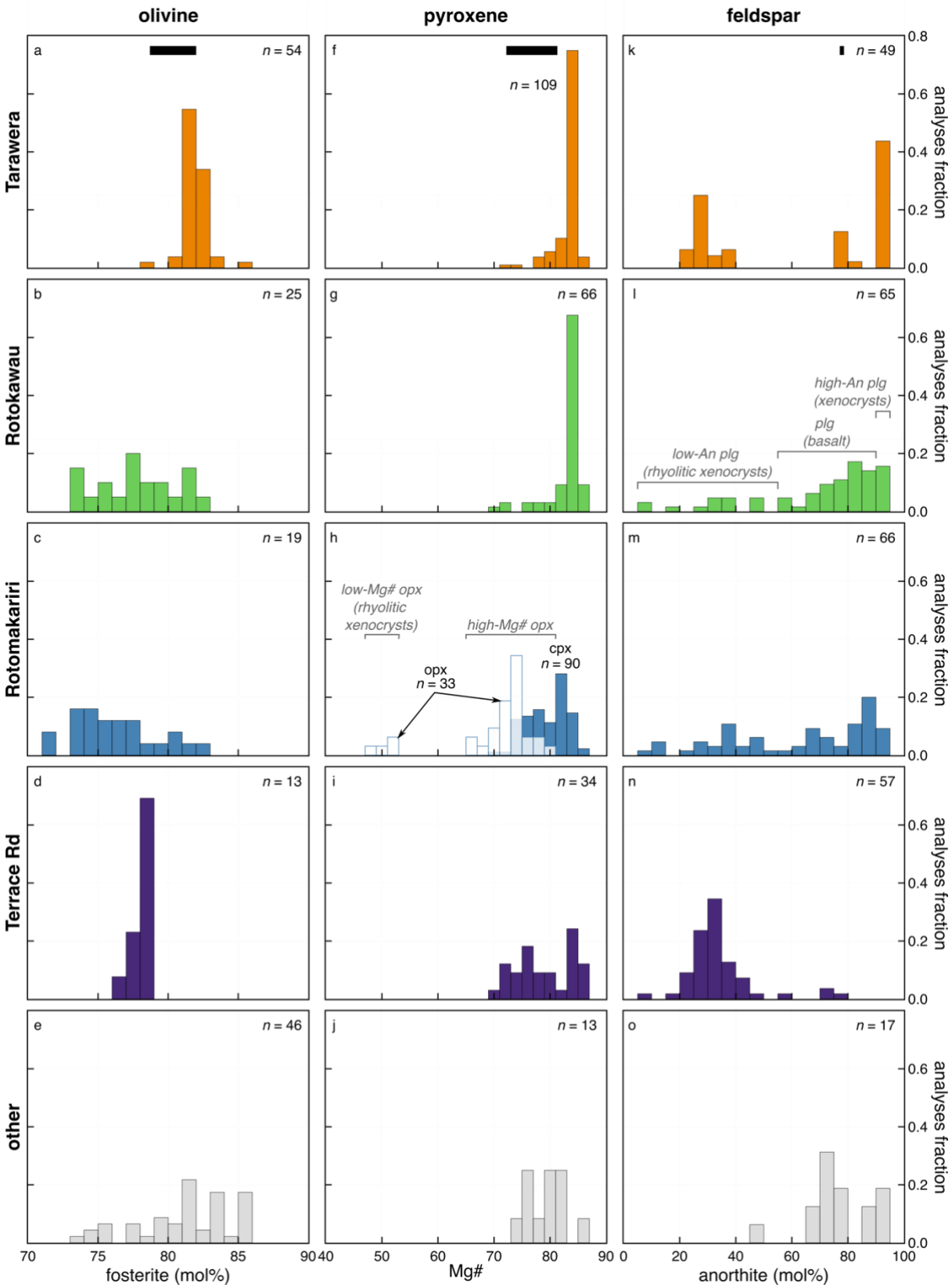


*Figure 3* Histograms of mineral chemistry showing fraction of crystal core analyses in each compositional bin (number of analyses *n* indicated for each panel). Each column represents a different mineral phase, labelled along the top: **(a–e)** olivine – forsterite content, **(f–j)** pyroxene – Mg# (filled bars are for cpx, unfilled bars in (h) are for opx, with different opx populations labelled in grey), and **(k–o)** plagioclase – anorthite content (different plg populations are labelled in grey in (l) but apply to all eruptions). Each row represents an individual eruption, which are labelled down the left-hand side and shown using colour: **(a, f, k)** Tarawera (orange), **(b, g, l)** Rotokawau (green), **(c, h, m)** Rotomakariri (blue), **(d, i, n)** Terrace Rd (purple), and **(e, j, o)** other OVC basalts (grey), which

includes Kaharoa, Rerewhakaaitu, Okareka, and Matahi. Range of microlite compositions from Rowe et al. (2021) for Tarawera shown as black bars in (a, f, k). *Data sources:* Matahi (Davis, 1985); Terrace Rd (Law et al., 2021; this study); Rotomakariri (Law et al., 2021; this study); Okareka (Barker et al., 2020; Shane et al., 2008); Rerewhakaaitu (Shane et al., 2007), Rotokawau (Beanland, 1989; Hiess et al., 2007; Law et al., 2021; this study); Kaharoa (Barker et al., 2020; Leonard et al., 2002), Tarawera (Barker et al., 2020; Hiess et al., 2007; Law et al., 2021; Rowe et al., 2021; this study).

### *4.2 Melt inclusions*

Most glass analyses in this study come from melt inclusions hosted in clinopyroxene, with minor orthopyroxene-hosted melt inclusion and groundmass glass analyses (Figure 4 and Figure 5; additional data are shown in Figure S7 of Supplementary Material). From our study, most glass analyses are from Tarawera, followed by Rotokawau then Rotomakariri, with a small number from Terrace Rd. The Tarawera dataset is supplemented with melt inclusion data from Barker et al. (2020) and Rowe et al. (2021).

Crystallisation, diffusion, and bubble-formation can alter major and volatile element chemistry of melt inclusions after entrapment (e.g., Barth et al., 2019; Barth and Plank, 2021; Bucholz et al., 2013; Danyushevsky et al., 2000, 1988; Dungan and Rhodes, 1978; Gaetani et al., 2012; Gaetani and Watson, 2002, 2000; Hartley et al., 2014, 2015; Lowenstern, 2003, 1995; Moore et al., 2015; Nielsen et al., 1998; Rasmussen et al., 2020; Roedder, 1979; Saper and Stolper, 2020; Schiano, 2003; Sobolev and Shimizu, 1993; Wallace et al., 2015). Based on mineral-melt exchange equilibria, most melt inclusions were not in equilibrium with their host crystal indicating post-entrapment crystallisation (PEC) has occurred (Figure S3a in Supplementary Material). The effects of PEC were corrected for using the method of Collins et al. (2022) and only data with <|15|% PEC-correction were used (see Supplementary Material for details).

Only the glass composition of melt inclusions was analysed; there was no attempt to account for volatiles contained in co-existing vapour bubbles (i.e., composition and size of vapour bubbles were not measured) to reconstruct bulk melt inclusion compositions. $CO_2$ is greatly affected by bubble formation, whilst $H_2O$, S, and Cl are less affected due to lower partitioning into the vapour phase and/or potential kinetic effects (e.g., Hartley et al., 2014; Maclennan, 2017; Moore et al., 2015; Rasmussen et al., 2020; Wallace et al., 2015). Rather than add additional uncertainty related to reconstructing the original melt composition, we assume $CO_2$ concentrations represent minimum estimates of the $CO_2$ content of the melt, and do not try and fit degassing trends to our data. Bulk (i.e., melt + bubble) $H_2O$ content can additionally be altered by diffusion into or out of the melt inclusion, which is discussed below (e.g., Barth et al., 2019; Barth and Plank, 2021; Bucholz et al., 2013; Gaetani et al., 2012; Hartley et al., 2015, 2014).

Melt inclusions and matrix glasses show a considerable range in composition (Figure 4a–c). Terrace Rd, Rotokawau, and Tarawera melt inclusions are predominantly basaltic to basaltic-andesite in composition, whereas Rotomakariri melt inclusions and matrix glasses range from basaltic andesite to dacitic (mostly andesitic). There are a small number of andesite-dacite melt inclusions from Tarawera and some matrix glass data from Tarawera and Rotokawau that are dacite-rhyolite. Basaltic to basaltic-andesite melt inclusions are similar in Terrace Rd, Rotokawau, and Tarawera, but were not found in Rotomakariri (Figure 4a–c). The most basaltic of these melt inclusions overlap with the higher $SiO_2$ range of the olivine-hosted melt inclusions from Barker et al. (2020) and some of these melt inclusions overlap with whole rock data (Figure 4a–c). There is a wide-range of $Al_2O_3$ at a given $SiO_2$ (15–19 wt% $Al_2O_3$ at 50 wt% $SiO_2$; Figure 4a). CaO decreases with increasing $SiO_2$, with some melt inclusions having higher CaO at a given $SiO_2$, overlapping with the whole rock data (Figure 4b). $K_2O$ increases with $SiO_2$ for both melt inclusions and whole rocks (Figure 4c).

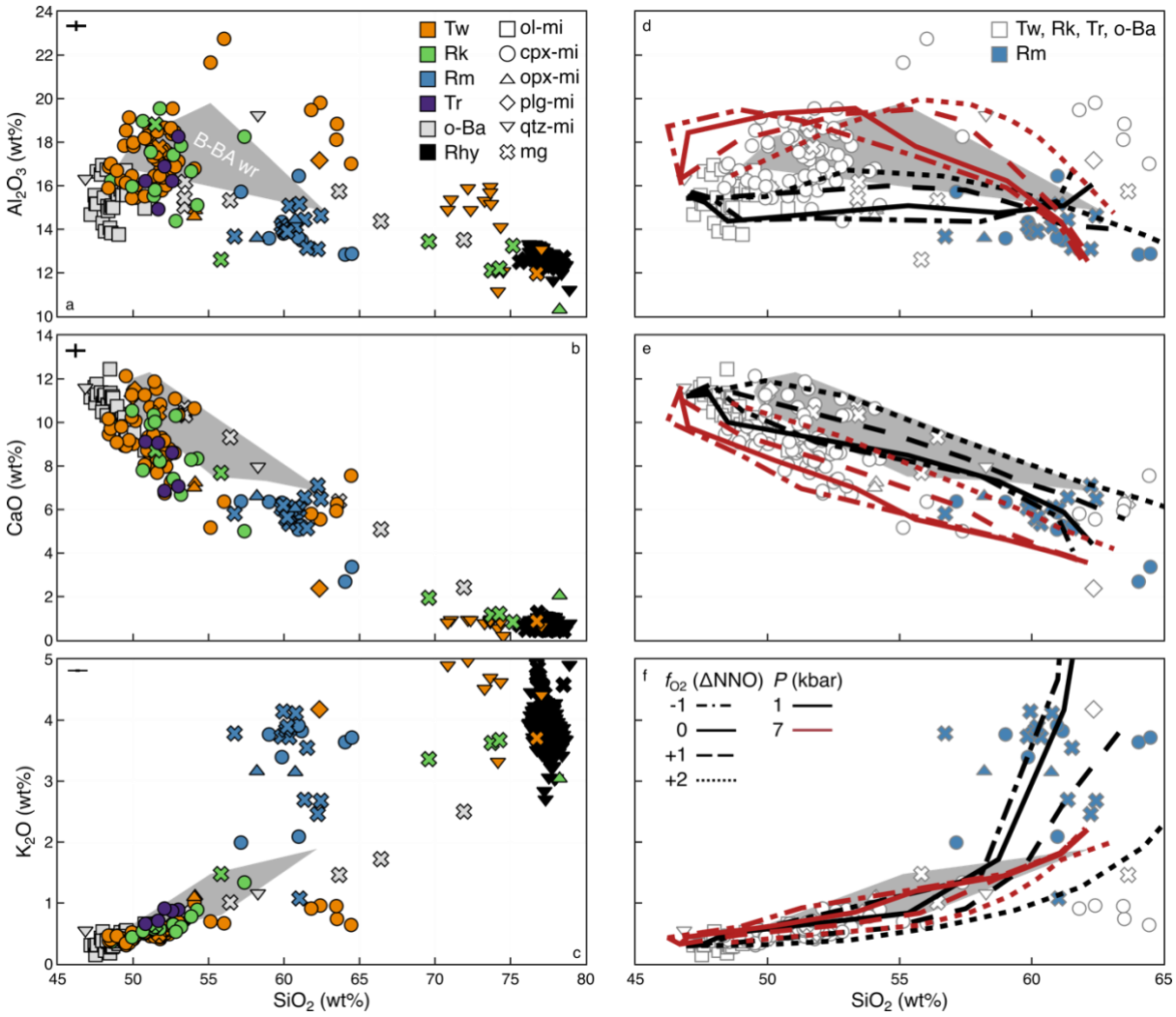


*Figure 4* Major element systematics for melt composition data for **(a)** $Al_2O_3$, **(b)** CaO, and **(c)** $K_2O$ vs. $SiO_2$. Symbol shapes distinguish between melt inclusion (PEC-corrected, hosted in olivine = square, clinopyroxene = circle, plagioclase = diamond, orthopyroxene = up-triangle, or quartz = down-triangle) and groundmass glass (cross). Different eruptions are indicated by symbol colour (Tarawera – Tw = orange, Rotokawau – Rk = green, Rotomakariri – Rm = blue, Terrace Rd – Tr = purple, other OVC basalts – o-Ba = grey, and OVC rhyolites – Rhy = black). The range in composition for whole rock data for basalt to basaltic-andesite OVC eruptions is shown by a grey field labelled "B-BA wr". Uncertainties for our data are indicated in the top-left corner of each panel and are two standard deviations of the precision based on repeat analyses of VG-2 over all analytical sessions (note the $K_2O$ error bar is small). In **(d–f)** the results from Rhyolite-MELTS modelling (note the reduced range of $SiO_2$ on the x-axis) is overlain on the melt data (white symbols with grey outlines are all data shown in (a–c) except Rotomakariri, which is shown in blue, and the whole rock data in the grey region). Calculations are from 1300 to 900 °C, 1 wt % $H_2O$ and 1000 ppm $CO_2$, 1 (black) or 7 (red) kbar, and various oxygen fugacity ($f_{O2}$: ΔNNO-1 dot-dash, 0 solid, +1 dash, and +2 dot) from a single melt composition. Additional data and results are shown in Figure S7 and S8 of Supplementary Material. *Data sources:* melt inclusion and groundmass glass for Terrace Road, Rotomakariri, and Rotokawau (this study); Tarawera melt inclusions hosted in clinopyroxene (this study; Rowe et al., 2021), olivine (Barker et al., 2020), plagioclase, orthopyroxene and quartz (Rowe et al., 2021); olivine-hosted melt inclusions for Okareka and Kaharoa (Barker et al., 2020); glass analyses from mafic blebs from Rerewhakaaitu (Shane et al., 2007); OVC basaltic whole rock (Beanland, 1989; Bowyer, 2001; Cole, 1979, 1973b; Gamble et al., 1993, 1990; Grange, 1937; Hiess et al., 2007; Leonard et al., 2002; Nairn, 1992, 1981, 1979; Nairn et al., 2004; Nairn, 2002; Pittari et al., 2016; Rooney and Deering, 2014; Rowe et al., 2021; Schmitz and Smith, 2004; Shane et al., 2008; Zellmer et al., 2020); and OVC rhyolitic melt inclusions and matrix glass (Johnson et al., 2011).

Basaltic to basaltic-andesite melt inclusions from Tarawera have a wide range in $H_2O$ contents (0–5 wt%), whereas Terrace Rd (2.0–4.4 wt%) and Rotokawau (0.8–3.1 wt%) have a more limited range (Figure 5a and e). The lack of correlation between $H_2O$ and $K_2O$ suggests

365 measured water contents are not primary (Figure 5e). Hence, crystallisation with volatile-
366 concentration or degassing has been overprinted by diffusive water-loss or -gain. Given the
367 large error in $H_2O$ measurements, it is difficult to discern between these processes; however,
368 the range in $H_2O$ is likely representative of the melt. Chlorine concentrations are lowest for
369 Terrace Rd (~1000–1100 ppm), then Tarawera (~850–1700 ppm); Rotokawau has the highest
370 (~1300–2300 ppm), which positively correlates with $K_2O$ (Figure 5b). Sulfur has a similarly
371 wide range in all three eruptions (~30–3300; Figure 5c) and fluorine concentrations are also
372 similar (~30–1000; Figure 5d), neither of which correlate with $K_2O$. $CO_2$ (433–756 ppm) was
373 measured for a subset of Tarawera melt inclusions only (Figure 5f). For S > 1000 ppm, S and
374 Cl positively correlate, whereas for S < 1000 ppm they negatively correlate (Figure 5g); S and
375 $H_2O$ show broad correlation (Figure 5h).

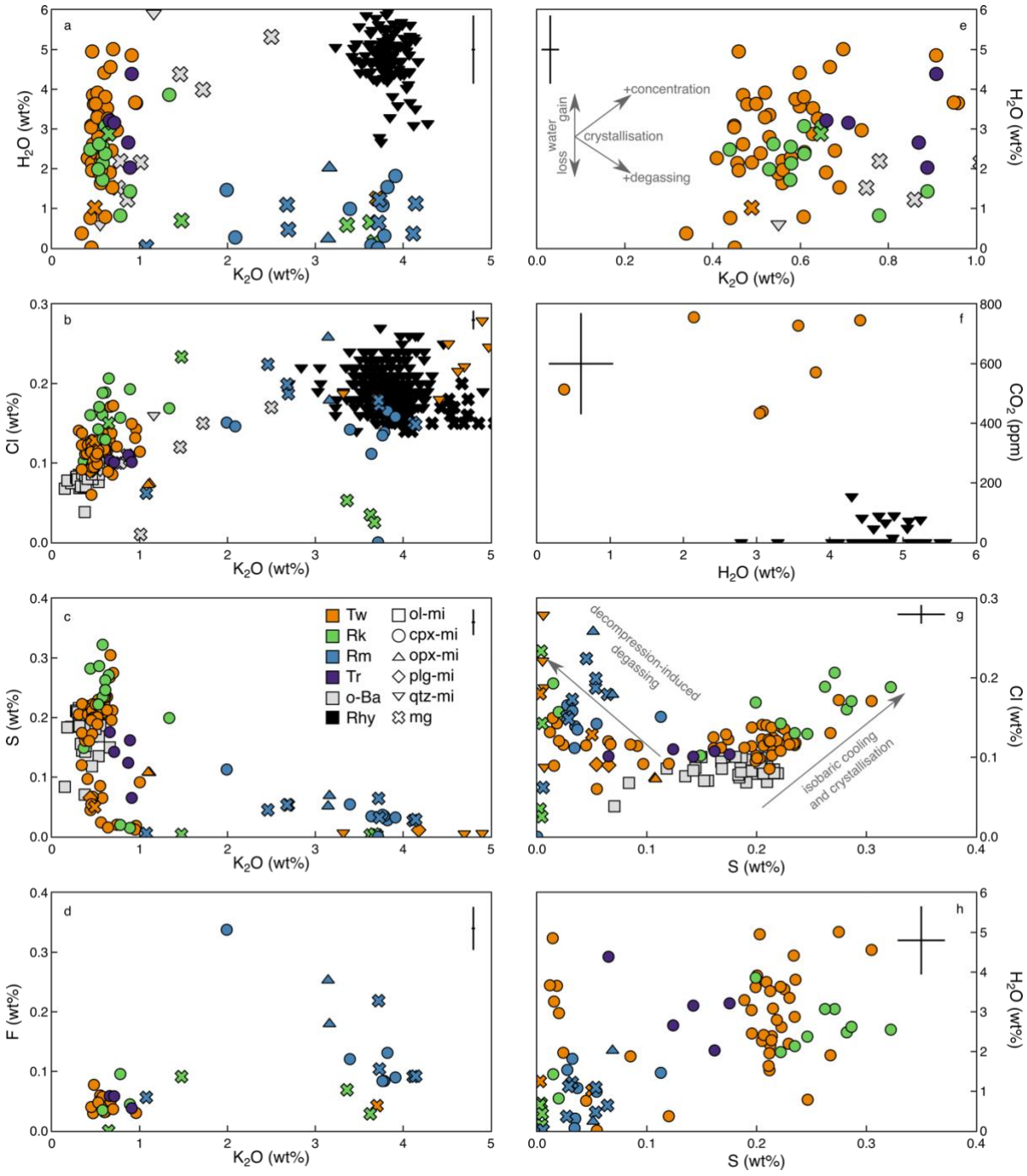


*Figure 5* Volatiles systematics for melt composition data for: **(a)** $H_2O$, **(b)** Cl, **(c)** S, **(d)** F, and **(e)** $H_2O$ (zoomed in scale compared to a) vs. $K_2O$; **(f)** $CO_2$ vs. $H_2O$; and **(g)** Cl and **(h)** $H_2O$ vs. S. Symbol shapes distinguish between melt inclusion (PEC-corrected, hosted in olivine = square, clinopyroxene, = circle plagioclase = diamond, orthopyroxene = up-triangle, or quartz = down-triangle) and groundmass glass (cross). Different eruptions are indicated by symbol colour (Tarawera – Tw = orange, Rotokawau – Rk = green, Rotomakariri – Rm = blue, Terrace Rd – Tr = purple, other OVC basalts – o-Ba = grey, and OVC rhyolites – Rhy = black). Uncertainties for our data are indicated in each panel as two standard deviations of precision based on repeat analyses of VG-2 over all analytical sessions for EPMA data (note the $K_2O$ error bar is small) or two standard deviations of the minimum precision based on repeat analyses of standards over all analytical sessions for SIMS data in (f). Trends for different processes are shown with grey arrows and labelled in (e) and (f). *Data sources:* melt inclusion and groundmass glass for Terrace Road, Rotomakariri, and Rotokawau (this study); Tarawera melt inclusions hosted in clinopyroxene (this study; Rowe et al., 2021), olivine (Barker et al., 2020), plagioclase, orthopyroxene and quartz (Rowe et al., 2021); olivine-hosted melt inclusions for Okareka and Kaharoa (Barker et al., 2020); glass analyses from mafic blebs from Rerewhakaaitu (Shane et al., 2007); and melt inclusions and groundmass glass from OVC rhyolites (Johnson et al., 2011).

Rotomakariri melt inclusions and groundmass glass are mostly andesitic, with low CaO and $Al_2O_3$ and high $K_2O$ (Figure 4a–c). The $H_2O$ and S contents of Rotomakariri melt inclusions are lower than most of the basaltic to basaltic-andesite melt inclusions, although similar to the low-sulfur (S <1000 ppm) set of clinopyroxene-hosted melt inclusions (Figure 5a and c). Chlorine is high and similar to Rotokawau (Figure 5b); fluorine is much higher than any of the basalts (Figure 5d). At Tarawera, a few clinopyroxene-hosted melt inclusions are also andesite-dacite, but have higher $Al_2O_3$, similar CaO, and lower $K_2O$ than Rotomakariri melt inclusions (Figure 4a–c). Dacite-rhyolite melt inclusions and groundmass glass are associated with orthopyroxene and quartz from Rotokawau and Tarawera (Figure 4a–c) and have low $H_2O$, variable Cl, very low S, and low F (Figure 5a–d).

# 5 Pre- and syn-eruptive storage, evolution, and mixing of multiple magmas

## *5.1 Similar basalts erupted in Tarawera, Terrace Rd, and Rotokawau*

### 5.1.1 Polybaric crystallisation and mixing

Most of the mineral and melt inclusion analyses in this study, namely clinopyroxene and their melt inclusions, $An_{50–90}$ plagioclase, and groundmass material were derived from basaltic magma (Figure 3 and Figure 4). Olivine compositions indicate these melts are not mantle-derived, but have already undergone prior crystallisation (Law et al., 2021). The spread in temperatures inferred from thermometry (Figure 6) suggests cooling-induced crystallisation is responsible for the compositional range of whole rock and melt inclusion data. The narrower spread in compositions and temperatures for whole rock and minerals compared to melt inclusions is consistent with the basaltic composition of the system. Conversely, melt inclusion compositions reflect local changes in temperature and associated crystallisation, recording snapshots of the melt present in a crystal-rich magma reservoir at depth. The mushy nature of this reservoir is further evidenced by abundant glomerocrysts in Terrace Rd, Rotomakariri, and Rotokawau (Figure 2i–n).

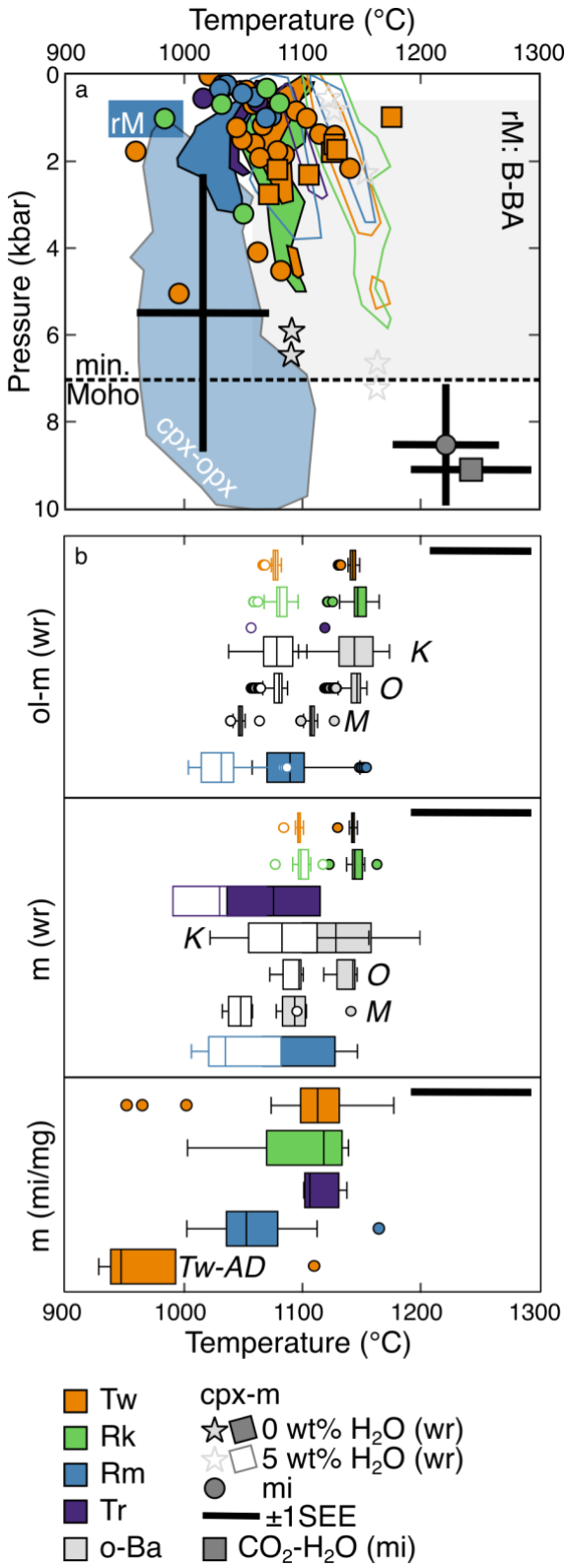


*Figure 6* Pressure and temperature estimates for each eruption (shown by colour, other OVC basalts include Kaharoa – *K*, Okareka – *O*, and Matahi – *M*). **(a)** Pressure vs. temperature from: cpx-m using whole rock data (coloured outlines are assuming 0 wt% $H_2O$ and filled regions are 5 wt%) and melt inclusion data (circles), where the standard errors of estimate (SEE) is shown in the bottom-right corner by the thick black lines with a circle in the middle; cpx-opx (labelled cpx-opx), where the SEE is shown by the thick black lines in the region; melt inclusion $CO_2$-$H_2O$ for minimum *P* and melt composition for *T* (squares), where the SEE is shown in the bottom-right corner by the thick black line with a square in the middle; and Rhyolite-MELTS modelling (regions labelled rM and rM: B-BA). Minimum depth of the TVZ Moho (Bannister et al., 2004) indicated by dashed black horizonal

line. **(b)** Box and whisker plots for temperature using ol-m and whole rock/melt inclusion/matrix glass composition. Estimates using whole rock compositions are shown assuming a melt composition that is anhydrous (filled) or $H_2O$-saturated (≤5 wt%, unfilled); measured $H_2O$ content is used for melt inclusions. The edges of the "box" are at the 1st and 3rd quartile of the data, with the median indicated by a horizontal line within the box. The "whiskers" extend out to the minimum and maximum data points within 1.5× the interquartile range (range between 1st and 2nd quartile) beyond the 1st and 3rd quartiles. Any outliers outside the whiskers are shown as individual data points (circles). The SEE for each thermometer is shown by the thick black line in the top-right of each panel. *Abbreviations*: ol = olivine, m = melt, wr = whole rock, cpx = clinopyroxene, mi = melt inclusion, and opx = orthopyroxene. Full descriptions of calculations given in Supplementary Material.

A wide range of pressures (~7 kbar to surface) is derived from melt-clinopyroxene barometry, with most estimates less than 3 kbar (Figure 6a). Based on volatile solubility, the $H_2O$-$CO_2$ measurements require some melts to be derived from at least 3 kbar (Figure 6a). These estimates overlap with pressure-temperature estimates for Tarawera from Rowe et al. (2021). The high $Al_2O_3$ requires plagioclase crystallisation to have been suppressed, suggesting differentiation at higher pressures (e.g., Blatter et al., 2013; Marxer et al., 2021; Müntener and Ulmer, 2018a; Nandedkar et al., 2014) or high water contents were preserved to low pressures (Rowe et al., 2021). Rhyolite-MELTS modelling is used to show that the compositions of melt inclusion and whole rock data do not correspond to fractional crystallisation at a unique pressure and oxygen fugacity (Figure 4d–f). Instead, the range in melt compositions is bracketed by fractional crystallisation during cooling (to 1050 °C) from a common, $H_2O$-saturated parent melt at relatively oxidised (ΔNNO=0 to +2) conditions at pressures between 1 and 7 kbar (Figure 4d–f and "rM: B-BA" region in Figure 6a). The oxygen fugacity range from Rhyolite-MELTS agrees with the limited literature whole rock $Fe^{3+}/Fe_T$ data (Grange, 1937; Cole, 1966; Nairn, 2002), which imply relatively oxidised conditions (~ΔNNO+1). Together these observations imply polybaric crystallisation of a single composition of basaltic magma (Figure 6a). Given the large model uncertainties (e.g., ±1.4 kbar for cpx-melt barometry; Putirka, 2008), individual magma reservoirs cannot be distinguished. However, the detailed mineral compositions (e.g., olivine; Figure 3a–e) and glomerocryst textures are distinct between eruptions (Figure 2i–n) indicating evolution in discrete, isolated pods prior to eruption, consistent with their known temporal and spatial spread.

The range in major element composition at a single $SiO_2$ (especially obvious in $Al_2O_3$; Figure 4d) is then a result of mixing between these basaltic magmas and their differentiated products. Interaction between basaltic magmas is also evidenced by the textures in the scoria, which indicate mixing between different batches of basalt with subtly different crystallisation conditions (i.e., come from different places in the magmatic system) or decompression histories (e.g., $T$–$H_2O$ conditions). At Tarawera, this includes the melt represented by the macrocryst-poor whole rock composition and the low/high-S melt inclusions (Figure 5g). A similar picture applies to Rotokawau, where mingled groundmass textures suggest multiple basaltic melts (Figure 2c). For Terrace Rd, the small glomerocrysts could be phenocrystic or antecrystic, whereas the large glomerocrysts are antecrystic and there is evidence for multiple melts in the groundmass (Figure 2e, i, and m). We interpret these observations in terms of evolution of a single, primitive, oxidised basalt magma in distinct, isolated, mushy pods due primarily to cooling-induced crystallisation, with some additional degassing and mixing during ascent of discrete magma batches.

#### 5.1.2 Volatiles contents and processes

$H_2O$ and $CO_2$ data are scattered, reflecting post-entrapment processes overprinting original magmatic conditions, such as bubble formation reducing $CO_2$ concentrations and H-diffusion modifying $H_2O$ (e.g., Barth et al., 2019; Barth and Plank, 2021; Bucholz et al., 2013; Gaetani

et al., 2012; Hartley et al., 2015, 2014; Maclennan, 2017; Moore et al., 2015; Rasmussen et al., 2020; Wallace et al., 2015) (Figure 5a, e, and f). The highest measured concentrations are ~5 wt% $H_2O$ and ~750 ppm $CO_2$, reflecting lower bounds on the $H_2O$-$CO_2$ concentrations of the magma. Measured water contents overlap with inferred melt water contents from melt inclusions and clinopyroxene H contents from Rowe et al. (2021).

Amphibole was not observed in the eruptions studied here. Amphibole has been described only in the groundmass of basaltic and gabbroic enclaves from the Kaharoa eruption, where amphibole crystallisation is thought to have been triggered by a late-stage increase in $H_2O$, possibly due to interaction with rhyolite (Leonard et al., 2002). Most of the melt inclusions at Tarawera, Rotokawau, and Terrace Rd record temperatures that are too high (>1050 °C) for amphibole stability despite their relatively high $H_2O$ concentrations (Figure 7) (Foden and Green, 1992). This suggests that basalt-rhyolite mixing prior to the Kaharoa eruption moved the magma into the amphibole stability field by cooling, rather than by increasing its $H_2O$ content.

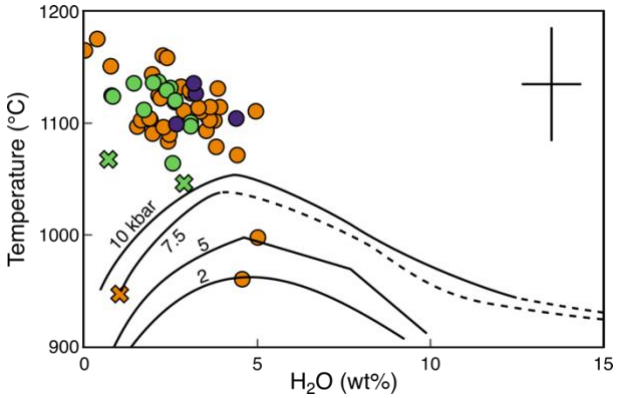


*Figure 7* Temperature vs. $H_2O$ for melt inclusion data (see Figure 4 for interpretation of the symbol shape and colour – only PEC-corrected data from this study are plotted). Temperature is derived from the melt composition and measured $H_2O$ concentration is plotted. Black curves are maximum temperatures amphibole is stable at for a given $H_2O$ content of the system from Foden and Green (1992) for different pressures (written on each line). Uncertainties are indicated for *T* (±1SEE) and $H_2O$ (±2 sd of the precision based on repeat analyses of secondary standard VG2) in the top-right corner.

The more primitive basaltic melt inclusions have elevated volatile concentrations compared to mid-ocean ridge basalts, reflecting the influence of a subducted slab component added to the mantle wedge source (Figure 5; e.g., Wysoczanski et al., 2006). The maximum volatile content of basaltic-andesite melt inclusions is similar ($H_2O$, Cl) or greatly exceed ($CO_2$, S) volatile concentrations in OVC rhyolites (Figure 5; e.g., Johnson et al., 2011). For Tarawera and Rotokawau, melt inclusions can be divided into two sub-groups based on S concentrations above and below ~1000 ppm (Figure 5g), which requires two separate crystallisation regimes as previously proposed by Rowe et al. (2021). We suggest that these regimes correspond to isobaric cooling and decompression-induced degassing (Figure 5g). Concentrations of S and Cl increase in the melt during crystallisation for melt inclusions with >1000 ppm S (Figure 5g). This behaviour indicates these elements behaved incompatibly (i.e., were not partitioned into crystallising minerals or exsolved fluids), such that fluid-melt bulk partition coefficients for S and Cl at these conditions were very low (e.g., Gennaro et al., 2021; O'Neill, 2020; Tattitch et al., 2021; Thomas and Wood, 2021). Rotokawau and Tarawera melt inclusions with <1000 ppm S show increasing Cl with decreasing S (Figure 5g). Decreasing pressure during ascent drives crystallisation and degassing, forming a fluid that sequesters S, but not Cl (e.g., Lesne et al., 2011).

### 5.1.3 Similar storage conditions and volatiles prior to eruptions of varying style

Despite the similar pre-eruptive compositions and conditions of the basaltic magma, there is a wide variation in eruption style (Figure 1b and Figure 6). Bamber et al. (2022, 2019) suggested moderate storage temperatures (<1100 °C) are important for generating basaltic plinian eruptions. These are shown to occur at Tarawera but are also found for the smaller intensity eruptions (Figure 6). Volatile concentrations ($H_2O$, Cl, and S) and trends are also similar between basaltic eruptions around the OVC (Figure 5). High $H_2O$ concentrations and $H_2O$ exsolution have been suggested to drive basaltic plinian eruptions (Bamber et al., 2019; Pérez et al., 2020). However, high $H_2O$ concentrations are found across the range of eruption styles at Okataina and are therefore not unique to Tarawera (Figure 5a and f). Both Rotokawau and Tarawera have a population of melt inclusions that have somewhat degassed (lower S contents), and this population may have been missed at Terrace Rd where fewer melt inclusions were analysed (Figure 5g). It has been suggested that melt inclusions from plinian eruptions record a unique degassing path (Moretti et al., 2018) compared to other explosive eruptions. Moretti et al. (2018) suggest lower Cl but higher S occurs in less explosive eruptions compared to more explosive eruptions due to the differences in dehydration and sulphide-saturation that occur during crystallisation. However, the observed differences in S and Cl concentration around the OVC do not relate to eruption style: Rotokawau has higher S and Cl but eruption intensity intermediate between Terrace Rd and Tarawera, and there is no evidence for sulphide-saturation (Figure 5g). High $CO_2$ concentrations are thought to be important for generating (sub-)plinian basaltic eruptions (e.g., Allison et al., 2021; Sable et al., 2009), which could be important around the OVC. Unfortunately, our $CO_2$ data for Tarawera are likely compromised by bubble formation and we do not have sufficient data to compare against smaller eruptions (Figure 5f).

External factors could also influence eruption style of basaltic magmas. Basaltic eruptions around the OVC are thought to be modulated by crustal faults. This is evidenced by the linear nature of their eruptive vents and that the dike orientations from the 1886 C.E. Tarawera eruption closely match the regional fault orientations (Nairn and Cole, 1981). There is also evidence of volcano-tectonic interactions for OVC rhyolitic eruptions (e.g., Berryman et al., 2022; Villamor et al., 2022). Hence, these eruptions may be triggered by earthquakes, especially given the high melt $H_2O$ contents and mushy-nature of storage (e.g., Hamling and Kilgour, 2020; Seropian et al., 2021). Additionally, the presence and physical state (e.g., viscosity) of large silicic bodies in the crust could affect basaltic eruption style by impeding (or not) the ascent of basaltic magmas to the surface. For instance, the lack of a low resistivity anomaly currently beneath Tarawera may suggest there was no large silicic body there during the 1886 A.D. eruption, allowing the basalt to erupt unimpeded (Bertrand et al, 2022). The presence of external water (e.g., lakes) will also modulate transitions from magmatic to phreatomagmatic eruption styles. Tectonics in addition to the complex nature of the crust around the OVC (and external water) may therefore be important for generating the wide variety of basaltic eruption styles observed.

### 5.1.4 Mixing and entrainment during ascent influenced by eruption style

Samples analysed in this study clearly point to variable extents of basaltic magma mixing prior to eruption (and also entrainment of xenocrystic high-An plagioclase described in Section 5.2). The implication is that a magma interacted with multiple different gabbroic bodies as it ascended through the crust, entraining crystals *en route*. This is also seen in differences in oxygen isotope compositions between crystals and groundmass in these eruptions (Law et al., *in review*). The timescales of interactions were likely very short (e.g., to preserve multiple

groundmass textures and produce the sharp rims of lower-An plagioclase around high-An plagioclase, Figure 2c and e–h), and probably occurred during pre-eruptive magma ascent. The proportion of crystals entrained is likely correlated with magma ascent rate, which potentially controls eruption style. Lower intensity eruptions (Terrace Road, Rotokawau) contain a high proportion of macrocrysts, whereas Tarawera has a negligible crystal cargo (0.5 vol%, Sable et al., 2009). The melt entrained more crystals as it passed through the mush layers in smaller eruptions than in the plinian eruption. This difference likely reflects the faster ascent rate of plinian magmas, rather than the cause *per se* of varying eruption style.

OVC basalts eruptions additionally show entrainment of rhyolitic material (e.g., low-Mg# orthopyroxene, low-An plagioclase, quartz, alkali feldspars, and rhyolitic melt inclusions), similar in composition to OVC rhyolitic eruptions (Figure 3 and Figure 4). Rhyolitic material appear to have been incorporated at a late-stage of magma ascent (e.g., sharp boundaries between basaltic and rhyolitic material, Figure 2p), probably when the basaltic magma ascended and briefly mingled with previously erupted, and relatively cold rhyolite domes (i.e., solid material in the crust or erupted at the surface, then buried).

The diversity of magma types and mixing dynamics evident in individual eruptions and across eruptions reflects the interplay between basaltic magma ascent rates and the distribution, composition, and rheological state of magma bodies both vertically and horizontally. As mixing timescales appear to be short, precursory signals to basaltic explosive eruptions could be limited, as recorded by the very short precursory signals observed in the days before the Tarawera 1886 C.E. eruption (Keam, 1988).

### *5.2 High-An plagioclase xenocyrsts*

High-An ($>An_{90}$) plagioclase grains are found in all OVC eruptions and basaltic material since ~55 ka, but also in basaltic material from the ~26.5 ka TVC Oruanui eruption (Allan et al., 2017; Rooyakkers et al., 2018; Wilson et al., 2006) and the ~330 ka OVC post-caldera deposits following the Matahina eruption (Deering et al., 2011). Therefore, these high-An plagioclase grains are preserved in spatially and temporally separated OVC (and TVC) basalts. To explain this ubiquity, these high-An plagioclase crystals must be derived from a common source or conditions. Thin, low-An rims surrounding high-An plagioclase indicates disequilibrium (Figure 2e–h), suggesting the high-An plagioclase are xenocrysts (Figure 3k–o). Additionally, $^{87}Sr/^{86}Sr$ ratios for high-An plagioclases are distinctly more radiogenic than the groundmass, affirming that they are derived from a separate source (Rowe et al., 2021). High-An plagioclase ($>An_{96}$) crystals are likely to have crystallised from most primitive TVZ basalts (Wilson et al., 2006; Zellmer et al., 2020), rather than melt inclusions or average whole rock compositions for each eruption (Figure 8; calculation details are given in Supplementary Material using Sisson and Grove, 1993).

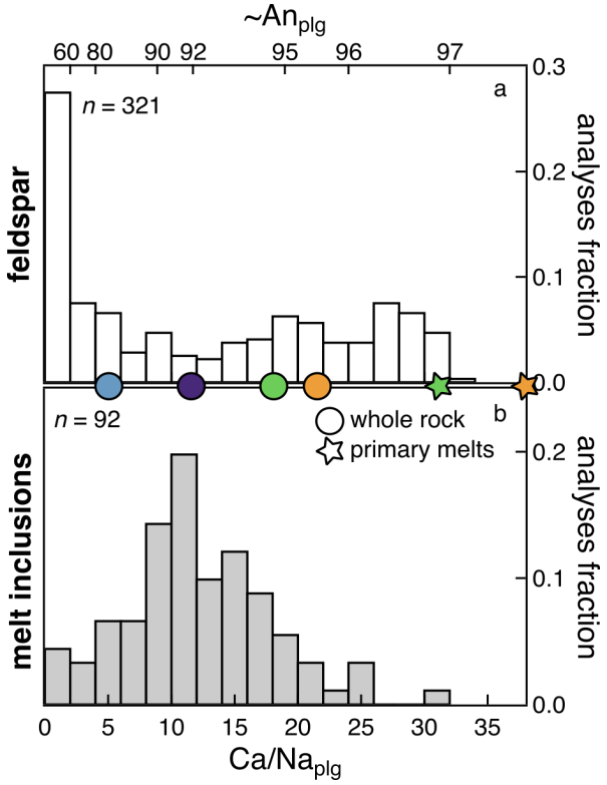


*Figure 8* Ca/Na ratios in plagioclase (and approximate An): **(a)** from all analysed grains; and **(b)** calculated for equilibrium with melt inclusions from this study. Symbols are calculated $Ca/Na_{plg}$ in equilibrium with average whole rock data for each eruption (circles) or primary melt compositions (stars) calculated by Zellmer et al. (2020), where symbol colour indicates eruption (Terrace Rd = purple, Rotomakariri = blue, Rotokawau = green, and Tarawera = orange). Equilibrium plagioclase compositions from melt compositions are calculated using Sisson and Grove (1993) (details in Supplementary Material)

High-An plagioclase can be indicative of hydrous conditions or crystallisation from Na-poor melts (e.g., Panjasawatwong et al., 1995; Takagi et al., 2005). High magmatic water contents would occur as melting is driven by fluid-fluxing of a fertile mantle in active calderas (e.g., Barker et al., 2020; Zellmer et al., 2020). Alternatively, the high-An content could be due to high Ca/Na in the melt and not reflect high water contents in the melt (e.g., Panjasawatwong et al., 1995); however, there is no evidence for melt with very high Ca/Na in the OVC. Inclusions of high-An plagioclase in clinopyroxene indicates plagioclase crystallisation before clinopyroxene, which occurs at lower $H_2O$. This may reflect the decompression melting source that is thought to dominate in intracaldera regions (Barker et al., 2020; Zellmer et al., 2020). Hence, decompression melting could also be a minor component of active calderas. However, further investigation is needed to distinguish between these different potential sources, in particular measuring melt inclusion compositions from these high-An plagioclase grains for volatiles and trace elements.

### *5.3 Rotomakariri*

Rotomakariri consists of mostly andesite melt inclusions and matrix glass, clinopyroxene, and high-Mg# orthopyroxene, but also olivine and both medium- and high-An plagioclase (Figure 3 and Figure 4). The high-An plagioclase are xenocrystic, as described in Section 5.2. Clinopyroxene-melt thermobarometry suggests crystallisation at 1050 ± 18 °C and 5 ± 3 kbar; two-pyroxene thermobarometry suggests higher pressures (~6 ± 4 kbar, with large model uncertainties of ±3.2 kbar) and overlapping temperatures (~950–1100 °C) (Figure 6). This is unusually hot for an andesite, although similar to Ruapehu and Whakaari andesites (~1000 °C;

Kilgour et al., 2021, 2013). Rhyolite-MELTS modelling indicates that the andesitic melt inclusions and matrix glass can form from a similar initial magma composition as the basalt characteristic of Tarawera, Terrace Rd, and Rotokawau. However, fractional crystallisation is to a lower *T* (~950 °C), shallower (1 kbar, well below two-pyroxene pressure estimates but within error of the clinopyroxene-melt barometry), and under more reducing conditions (ΔNNO-1 to 0) than those that generated the basaltic-andesites (Figure 4d–f).

Rotomakariri melt inclusion $H_2O$ contents are very low, but this could indicate diffusive loss of $H_2O$, which is supported by many Rotomakariri melt inclusions being crystallised (these were not analysed; Figure 5a). The low Cl and S concentrations indicate partitioning into a coexisting fluid (Figure 5b, c, and g). This is expected at low pressures and the hot, dry melt conditions observed; especially for S in more evolved melt compositions (e.g., Clemente et al., 2004; Gennaro et al., 2021; O'Neill, 2020; Tattitch et al., 2021; Thomas and Wood, 2021). Overall, this suggests Rotomakariri was a basaltic magma like Tarawera, Terrace Rd, and Rotokawau, which had entrained xenocrystic high-An plagioclase. It then stalled at shallow levels, resulting in low volatile contents and further cooling, crystallising to an andesite melt composition prior to eruption.

## 6 The magmatic architecture around the OVC

The mineral and melt inclusion compositions measured in Tarawera, Terrace Rd, Rotokawau and Rotomakariri are common to many different OVC eruptions. For instance, similar melt inclusions (albeit more primitive) and mineral chemistries are found in other basalts from around the OVC (e.g., Kaharoa, Okareka, Matahi, and Matahina) and even in TVC basaltic material (e.g., Oraunui), showing that these are common features within the TVZ (Allan et al., 2017; Barker et al., 2020; Deering et al., 2011; Rooyakkers et al., 2018; Wilson et al., 2006). As the same basaltic magmas are occurring in eruptions separated spatially and temporally, these sets of conditions must be common around the OVC even though magmas themselves were not sourced from the same spatio-temporal reservoirs.

Combining the evidence from barometry and mixing textures suggests a crust full of individual magma reservoirs around the OVC, that are variously sampled during eruption. Despite large model uncertainties, pressures derived from clinopyroxene-melt and $H_2O$-$CO_2$ barometery and rhyolite-MELTS modelling lie within the TVZ crust assuming a crustal density of 2700 $kg \cdot m^{-3}$ and a Moho at 25–30 km or 7–8 kbar pressure (Bannister et al., 2004). This suggests that basaltic magmas, in addition to rhyolitic magmas, are stored and evolve polybarically within the crust. This agrees with current geochemical and geophysical constraints from previous Tarawera clinopyroxene barometry (1–3 kbar, with some >7 kbar, reported in Sable et al., 2009) and the presence of partial melt bodies at similar depths around the OVC, such as at 6–16 km using receiver functions (Bannister et al., 2004), 10–20 km (as shallow as 8 km beneath Waimungu) using electrical resistivity inversions (Heise et al., 2016, 2010), 8–10 km from earthquake swarms attributed to a basaltic dike intrusion (Benson et al., 2021), 5–8 km from lower P-wave velocities (Bannister et al., 2022), and 8–15 km for a complex of relatively mafic magma from magnetotelluric models (Bertrand et al., 2022). Additionally, conceptual models based on petrological modelling invoke mafic sheets residing at 11–15 km, with some isolated pods found at 8–6 km depths (Cole et al., 2014; Deering et al., 2010). Large uncertainties in clinopyroxene-melt barometry mean individual magma reservoirs cannot be identified using this method. However, the mineral textures and compositions suggest evolution in isolated reservoirs, where each batch has its own distinct composition reflecting their individual histories.

These observations suggest that a thick, crustal mush – containing a wealth of individual, isolated pockets of magmas – is mostly trapping the ascending basalts in the crust that fuel magmatism around the OVC. This model likely applies more generally to active calderas in the TVZ and is similar to other arc settings, such as the Andean Puna plateau, resulting in the dominance of compositionally-evolved volcanism (e.g., Delph et al., 2017; Kay et al., 2010). However, the extensional regime of the TVZ is clearly important in allowing some of these basalts to reach the surface and erupt explosively.

The few basalts that do make it to the surface have passed through the complicated crustal mush and carry the signature of these interactions in their crystal cargo. This highlights the use of basaltic mineral and melt inclusion chemistry as windows into the sub-surface in silicic magmatic regions, extending its application from using olivine-hosted melt inclusions to understand mantle melting dynamics (e.g., Barker et al., 2020) to analysing clinopyroxene-hosted melt inclusions to gain insight into crustal processes. Combining data from multiple eruptions separated spatially and temporally has highlighted that similar processes are important around the OVC for potentially the last ~30 ka.

## 7 Author Contributions

ECH, JDB, HMM, and GK conceived the project idea. ECH and SL collected and processed the data. All authors contributed to data interpretation. ECH led manuscript production with further contribution from all authors.

## 8 Acknowledgements

We would like to thank the Ruawahia 2B trust for welcoming us onto Mount Tarawera and permitting us to collect samples on the mountain and especially Ken Raureti, Tīpene Marr, and Paul Warbrick for their support of this work; Kaingaroa Timberlands for permits to access Kaingaroa Forest and Waimangu Forest to collect samples; Yves Feisel (now at the University of Mainz, Germany), Marco Michelini (now at the University of Pittsburgh, USA), Brad Scott (Te Pū Ao | GNS Science, Aotearoa New Zealand), and Nick Macdonald (Te Pū Ao | GNS Science, Aotearoa New Zealand) for helping with sample collection; Richard Hinton for his assistance at the NERC ion microprobe facility at the University of Edinburgh, UK (IMF560/0515); Stuart Kearns and Ben Buse for their assistance with the electron probe and SEM at the University of Bristol, UK; three anonymous reviewers for their constructive reviews that improved the clarity and interpretation of the paper; and Prof. Mike Rowe (University of Auckland, Aotearoa New Zealand) for their editorial handling of the paper and comments that greatly improved the paper. ECH was supported by a NERC GW4+ DTP studentship (NE/L002434/1) and is thankful for the support and additional funding from CASE partner Te Pū Ao | GNS Science, Aotearoa New Zealand, and a Geology Option Post-Doctoral Fellowship from Caltech, CA USA. SL was supported by a NERC $E^3$ DTP studentship (NE/L002558/1). GK and ECH are supported by the Hazards and Risk Management Programme, which is part of New Zealand Strategic Science Investment Funding (SSIF) from the New Zealand Ministry of Business, Innovation & Employment (MBIE). JDB acknowledges support through a Royal Society Research Professorship.

## 9 References

Allan, A.S.R., Barker, S.J., Millet, M.A., Morgan, D.J., Rooyakkers, S.M., Schipper, C.I., Wilson, C.J.N., 2017. A cascade of magmatic events during the assembly and eruption of a super-sized magma body. Contrib. to

Mineral. Petrol. 172, 49. https://doi.org/10.1007/s00410-017-1367-8
Allison, C.M., Roggensack, K., Clarke, A.B., 2021. Highly explosive basaltic eruptions driven by CO2 exsolution. Nat. Commun. 12, 217. https://doi.org/10.1038/s41467-020-20354-2
Annen, C., Blundy, J.D., Sparks, R.S.J., 2006. The Genesis of Intermediate and Silicic Magmas in Deep Crustal Hot Zones. J. Petrol. 47, 505–539. https://doi.org/10.1093/petrology/egi084
Bamber, E.C., Arzilli, F., Polacci, M., Hartley, M.E., Fellowes, J., Di Genova, D., Chavarría, D., Saballos, J.A., Burton, M.R., 2019. Pre- and syn-eruptive conditions of a basaltic Plinian eruption at Masaya Volcano, Nicaragua: The Masaya Triple Layer (2.1 ka). J. Volcanol. Geotherm. Res. 106761. https://doi.org/10.1016/J.JVOLGEORES.2019.106761
Bamber, E.C., La Spina, G., Arzilli, F., de, M., Vitturi, M., Polacci, M., Hartley, M.E., Petrelli, M., Fellowes, J., Burton, M., 2022. Basaltic Plinian eruptions at Las Sierras-Masaya volcano driven by cool storage of crystal-rich magmas. Commun. Earth Environ. 2022 31 3, 1–17. https://doi.org/10.1038/s43247-022-00585-5
Bannister, S., Bertrand, E.A., Heimann, S., Bourguignon, S., Asher, C., Shanks, J., Harvison, A., 2022. Imaging sub-caldera structure with local seismicity, Okataina Volcanic Centre, Taupo Volcanic Zone, using double-difference seismic tomography. J. Volcanol. Geotherm. Res. 431, 107653. https://doi.org/10.1016/J.JVOLGEORES.2022.107653
Bannister, S.C., Bryan, C.J., Bibby, H.M., 2004. Shear wave velocity variation across the Taupo Volcanic Zone, New Zealand, from receiver function inversion. Geophys. J. Int. 159, 291–310. https://doi.org/10.1111/j.1365-246X.2004.02384.x
Barker, S.J., Rowe, M.C., Wilson, C.J.N., Gamble, J.A., Rooyakkers, S.M., Wysoczanski, R.J., Illsley-Kemp, F., Kenworthy, C.C., 2020. What lies beneath? Reconstructing the primitive magmas fueling voluminous silicic volcanism using olivine-hosted melt inclusions. Geology 48, 504–508. https://doi.org/10.1130/G47422.1
Barth, A., Newcombe, M., Plank, T., Gonnermann, H., Hajimirza, S., Soto, G.J., Saballos, A., Hauri, E., 2019. Magma decompression rate correlates with explosivity at basaltic volcanoes — Constraints from water diffusion in olivine. J. Volcanol. Geotherm. Res. 387, 106664. https://doi.org/10.1016/j.jvolgeores.2019.106664
Barth, A., Plank, T., 2021. The Ins and Outs of Water in Olivine-Hosted Melt Inclusions: Hygrometer vs. Speedometer. Front. Earth Sci. 9, 343. https://doi.org/10.3389/feart.2021.614004
Beanland, S., 1989. The Rotokawau Basalt. University of Otago.
Beanland, S., Houghton, B.F., 1978. Rotokawau Tephra : basaltic maars in Okataina Volcanic Centre, Taupo volcanic zone. New Zeal. Geol. Surv. Bull. 37–43.
Benson, T.W., Illsley-Kemp, F., Elms, H.C., Hamling, I.J., Savage, M.K., Wilson, C.J.N., Mestel, E.R.H., Barker, S.J., 2021. Earthquake Analysis Suggests Dyke Intrusion in 2019 Near Tarawera Volcano, New Zealand. Front. Earth Sci. 8, 604. https://doi.org/10.3389/feart.2020.606992
Berryman, K., Villamor, P., Nairn, I., Begg, J., Alloway, B. V., Rowland, J., Lee, J., Capote, R., 2022. Volcano-tectonic interactions at the southern margin of the Okataina Volcanic Centre, Taupō Volcanic Zone, New Zealand. J. Volcanol. Geotherm. Res. 427, 107552. https://doi.org/10.1016/J.JVOLGEORES.2022.107552
Bertrand, E.A., Kannberg, P., Caldwell, T.G., Heise, W., Constable, S., Scott, B., Bannister, S., Kilgour, G., Bennie, S.L., Hart, R., Palmer, N., 2022. Inferring the magmatic roots of volcano-geothermal systems in the Rotorua Caldera and Okataina Volcanic Centre from magnetotelluric models. J. Volcanol. Geotherm. Res. 431, 107645. https://doi.org/10.1016/J.JVOLGEORES.2022.107645
Blatter, D.L., Sisson, T.W., Hankins, W. Ben, 2013. Crystallization of oxidized, moderately hydrous arc basalt at mid- to lower-crustal pressures: implications for andesite genesis. Contrib. to Mineral. Petrol. 166, 861–886. https://doi.org/10.1007/s00410-013-0920-3
Bowyer, D.A., 2001. Petrologic, Geochemical and Isotopic Evolution of Rhyolite Lavas from the Okataina, Rotorua and Kapenga Volcanic Centres, Taupo Volcanic Zone, New Zealand. University of Waikato.
Bucholz, C.E., Gaetani, G.A., Behn, M.D., Shimizu, N., 2013. Post-entrapment modification of volatiles and oxygen fugacity in olivine-hosted melt inclusions. Earth Planet. Sci. Lett. 374, 145–155. https://doi.org/10.1016/j.epsl.2013.05.033
Buck, C.E., Higham, T.F.G., Lowe, D.J., 2003. Bayesian tools for tephrochronology: http://dx.doi.org/10.1191/0959683603hl652ft 13, 639–647. https://doi.org/10.1191/0959683603HL652FT
Burt, R.M., Brown, S.J.A., Cole, J.W., Shelley, D., Waight, T.E., 1998. Glass-bearing plutonic fragments from ignimbrites of the Okataina caldera complex, Taupo Volcanic Zone, New Zealand: remnants of a partially molten intrusion associated with preceding eruptions. J. Volcanol. Geotherm. Res. 84, 209–237. https://doi.org/10.1016/S0377-0273(98)00039-0
Carey, R.J., Houghton, B.F., Sable, J.E., Wilson, C.J.N., 2007. Contrasting grain size and componentry in complex proximal deposits of the 1886 Tarawera basaltic Plinian eruption. Bull. Volcanol. 69, 903–926. https://doi.org/10.1007/s00445-007-0117-6

Clemente, B., SCAILLET, B., PICHAVANT, M., 2004. The Solubility of Sulphur in Hydrous Rhyolitic Melts. J. Petrol. 45, 2171–2196. https://doi.org/10.1093/petrology/egh052
Cole, J.W., 1979. Structure, petrology, and genesis of Cenozoic volcanism, Taupo Volcanic Zone, New Zealand—a review. New Zeal. J. Geol. Geophys. 22, 631–657. https://doi.org/10.1080/00288306.1979.10424173
Cole, J.W., 1973a. High-alumina basalts of Taupo Volcanic Zone, New Zealand. Lithos 6, 53–64. https://doi.org/10.1016/0024-4937(73)90079-0
Cole, J.W., 1973b. High-alumina basalts of Taupo Volcanic Zone, New Zealand. LITHOS 6, 53–64. https://doi.org/10.1016/0024-4937(73)90079-0
Cole, J.W., 1970a. Structure and eruptive history of the Tarawera Volcanic Complex. New Zeal. J. Geol. Geophys. 13, 879–902. https://doi.org/10.1080/00288306.1970.10418208
Cole, J.W., 1970b. Petrology of the basic rocks of the Tarawera Volcanic Complex. New Zeal. J. Geol. Geophys. 13, 925–936. https://doi.org/10.1080/00288306.1970.10418210
Cole, J.W., Deering, C.D., Burt, R.M., Sewell, S., Shane, P.A., Matthews, N.E., 2014. Okataina Volcanic Centre, Taupo Volcanic Zone, New Zealand: A review of volcanism and synchronous pluton development in an active, dominantly silicic caldera system. Earth-Science Rev. 128, 1–17. https://doi.org/10.1016/j.earscirev.2013.10.008
Collins, N., Rowe, M.C., Kilgour, G., Nichols, A.R.L., Schipper, C.I., Tari, D., Garaebiti, E., 2022. A Petrologic Insight into Transitioning Eruption Styles from the Devil's Rock Region, Ambae, Vanuatu. J. Petrol. 63, 1–22. https://doi.org/10.1093/PETROLOGY/EGAC050
Danyushevsky, L., Della-Pasqua, F.N., Sokolov, S., 2000. Re-equilibration of melt inclusions trapped by magnesian olivine phenocrysts from subduction-related magmas: Petrological implications. Contrib. to Mineral. Petrol. 138, 68–83. https://doi.org/10.1007/PL00007664
Danyushevsky, L., Sobolev, A.V., Dmitriev, L.V., 1988. Orthopyroxene-bearing low-Ti tholeiites: The new type of ceanic ridge tholeiite. Trans. USSR Acad. Sci. Earth Sci. Sect. 292, 102–105.
Darragh, M.B., Cole, J.W., Nairn, I.A., Shane, P.A., 2006. Pyroclastic stratigraphy and eruption dynamics of the 21.9 ka Okareka and 17.6 ka Rerewhakaaitu eruption episodes from Tarawera Volcano, Okataina Volcanic Centre, New Zealand. New Zeal. J. Geol. Geophys. 49, 309–328. https://doi.org/10.1080/00288306.2006.9515170
Davis, W.J., 1985. Geochemistry and petrology of the Rotoiti and Earthquake Flat pyroclastic deposits. University of Auckland.
Deering, C.D., Cole, J.W., Vogel, T.A., 2011. Extraction of crystal-poor rhyolite from a hornblende-bearing intermediate mush: A case study of the caldera-forming Matahina eruption, Okataina volcanic complex. Contrib. to Mineral. Petrol. 161, 129–151. https://doi.org/10.1007/s00410-010-0524-0
Deering, C.D., Gravley, D.M., Vogel, T.A., Cole, J.W., Leonard, G.S., 2010. Origins of cold-wet-oxidizing to hot-dry-reducing rhyolite magma cycles and distribution in the Taupo Volcanic Zone, New Zealand. Contrib. to Mineral. Petrol. 160, 609–629. https://doi.org/10.1007/s00410-010-0496-0
Delph, J.R., Ward, K.M., Zandt, G., Ducea, M.N., Beck, S.L., 2017. Imaging a magma plumbing system from MASH zone to magma reservoir. Earth Planet. Sci. Lett. 457, 313–324. https://doi.org/10.1016/J.EPSL.2016.10.008
Ducea, M.N., Saleeby, J.B., Bergantz, G., 2015. The Architecture, Chemistry, and Evolution of Continental Magmatic Arcs. http://dx.doi.org/10.1146/annurev-earth-060614-105049 43, 299–331. https://doi.org/10.1146/ANNUREV-EARTH-060614-105049
Dungan, M.A., Rhodes, J.M., 1978. Residual glasses and melt inclusions in basalts from DSDP Legs 45 and 46: Evidence for magma mixing. Contrib. to Mineral. Petrol. 67, 417–431. https://doi.org/10.1007/BF00383301
Foden, J.D., Green, D.H., 1992. Possible role of amphibole in the origin of andesite: some experimental and natural evidence. Contrib. to Mineral. Petrol. 109, 479–493. https://doi.org/10.1007/BF00306551
Froggatt, P.C., Lowe, D.J., 1990. A review of late Quaternary silicic and some other tephra formations from New Zealand: Their stratigraphy, nomenclature, distribution, volume, and age. New Zeal. J. Geol. Geophys. 33, 89–109. https://doi.org/10.1080/00288306.1990.10427576
Gaetani, G.A., O'Leary, J.A., Shimizu, N., Bucholz, C.E., Newville, M., 2012. Rapid reequilibration of H2O and oxygen fugacity in olivine-hosted melt inclusions. Geology 40, 915–918. https://doi.org/10.1130/G32992.1
Gaetani, G.A., Watson, E.B., 2002. Modeling the major-element evolution of olivine-hosted melt inclusions. Chem. Geol. 183, 25–41. https://doi.org/10.1016/S0009-2541(01)00370-9
Gaetani, G.A., Watson, E.B., 2000. Open system behavior of olivine-hosted melt inclusions. Earth Planet. Sci. Lett. 183, 27–41. https://doi.org/10.1016/S0012-821X(00)00260-0
Gamble, J.A., Smith, I.E.M., Graham, I.J., Peter Kokelaar, B., Cole, J.W., Houghton, B.F., Wilson, C.J.N., 1990. The petrology, phase relations and tectonic setting of basalts from the taupo volcanic zone, New

Zealand and the Kermadec Island arc - havre trough, SW Pacific. J. Volcanol. Geotherm. Res. 43, 253–270. https://doi.org/10.1016/0377-0273(90)90055-K
Gamble, J.A., Smith, I.E.M., McCulloch, M.T., Graham, I.J., Kokelaar, B.P., 1993. The geochemistry and petrogenesis of basalts from the Taupo Volcanic Zone and Kermadec Island Arc, S.W. Pacific. J. Volcanol. Geotherm. Res. 54, 265–290. https://doi.org/10.1016/0377-0273(93)90067-2
Gennaro, E., Paonita, A., Iacono-Marziano, G., Moussallam, Y., Pichavant, M., Peters, N., Martel, C., 2020. Sulphur Behaviour and Redox Conditions in Etnean Magmas during Magma Differentiation and Degassing. J. Petrol. 61, egaa095. https://doi.org/10.1093/PETROLOGY/EGAA095
Ghiorso, M.S., Gualda, G.A.R., 2015. An H2O–CO2 mixed fluid saturation model compatible with rhyolite-MELTS. Contrib. to Mineral. Petrol. 169, 53. https://doi.org/10.1007/s00410-015-1141-8
Graham, I.J., Cole, J.W., Briggs, R.M., Gamble, J.A., Smith, I.E.M., 1995. Petrology and petrogenesis of volcanic rocks from the Taupo Volcanic Zone: a review. J. Volcanol. Geotherm. Res. 68, 59–87. https://doi.org/10.1016/0377-0273(95)00008-I
Grange, L.I., 1937. The geology of the Rotorua-Taupo Subdivision, Rotorua and Kaimanawa Divisions. New Zeal. Geol. Surv. Bull. 37, 1–138.
Grove, T.L., Till, C.B., Krawczynski, M.J., 2012. The Role of H2O in Subduction Zone Magmatism. http://dx.doi.org/10.1146/annurev-earth-042711-105310 40, 413–439. https://doi.org/10.1146/ANNUREV-EARTH-042711-105310
Gualda, G.A.R., Ghiorso, M.S., Lemons, R. V., Carley, T.L., 2012. Rhyolite-MELTS: a Modified Calibration of MELTS Optimized for Silica-rich, Fluid-bearing Magmatic Systems. J. Petrol. 53, 875–890. https://doi.org/10.1093/PETROLOGY/EGR080
Hamling, I.J., Kilgour, G., 2020. Goldilocks conditions required for earthquakes to trigger basaltic eruptions: Evidence from the 2015 Ambrym eruption. Sci. Adv. 6, eaaz5261. https://doi.org/10.1126/SCIADV.AAZ5261
Hamling, I.J., Kilgour, G., Hreinsdóttir, S., Bertrand, E., Bannister, S., 2022. Estimating the distribution of melt beneath the Okataina Caldera, New Zealand: An integrated approach using geodesy, seismology and magnetotellurics. J. Volcanol. Geotherm. Res. 426, 107549. https://doi.org/10.1016/J.JVOLGEORES.2022.107549
Hartley, M.E., Maclennan, J., Edmonds, M., Thordarson, T., 2014. Reconstructing the deep CO2 degassing behaviour of large basaltic fissure eruptions. Earth Planet. Sci. Lett. 393, 120–131. https://doi.org/10.1016/j.epsl.2014.02.031
Hartley, M.E., Neave, D.A., Maclennan, J., Edmonds, M., Thordarson, T., 2015. Diffusive over-hydration of olivine-hosted melt inclusions. Earth Planet. Sci. Lett. 425, 168–178. https://doi.org/10.1016/J.EPSL.2015.06.008
Heise, W., Caldwell, T.G., Bertrand, E.A., Hill, G.J., Bennie, S.L., Palmer, N.G., 2016. Imaging the deep source of the Rotorua and Waimangu geothermal fields, Taupo Volcanic Zone, New Zealand. J. Volcanol. Geotherm. Res. 314, 39–48. https://doi.org/10.1016/j.jvolgeores.2015.10.017
Heise, W., Caldwell, T.G., Bibby, H.M., Bennie, S.L., 2010. Three-dimensional electrical resistivity image of magma beneath an active continental rift, Taupo Volcanic Zone, New Zealand. Geophys. Res. Lett. 37, n/a-n/a. https://doi.org/10.1029/2010GL043110
Hiess, J., Cole, J.W., Spinks, K.D., 2007. Influence of the crust and crustal structure on the location and composition of high-alumina basalts of the Taupo Volcanic Zone, New Zealand. New Zeal. J. Geol. Geophys. 50, 327–342. https://doi.org/10.1080/00288300709509840
Hogg, A.G., Higham, T.F.G., Lowe, D.J., Palmer, J.G., Reimer, P.J., Newnham, R.M., 2003. A wiggle-match date for Polynesian settlement of New Zealand. Antiquity 77, 116–125. https://doi.org/10.1017/S0003598X00061408
Hopkins, J.L., Lowe, D.J., Horrocks, J.L., 2021. Tephrochronology in Aotearoa New Zealand. https://doi.org/10.1080/00288306.2021.1908368 64, 153–200. https://doi.org/10.1080/00288306.2021.1908368
Houghton, B.F., Hackett, W.R., 1984. Strombolian and phreatomagmatic deposits of Ohakune craters, Ruapehu, New Zealand: A complex interaction between external water and rising basaltic magma. J. Volcanol. Geotherm. Res. 21, 207–231. https://doi.org/10.1016/0377-0273(84)90023-4
Houghton, B.F., Wilson, C.J.N., McWilliams, M.O., Lanphere, M.A., Weaver, S.D., Briggs, R.M., Pringle, M.S., 1995. Chronology and dynamics of a large silicic magmatic system: central Taupo Volcanic Zone, New Zealand. Geology 23, 13–16. https://doi.org/10.1130/0091-7613(1995)023<0013:CADOAL>2.3.CO;2
Hughes, E.C., Buse, B., Kearns, S.L., Blundy, J.D., Kilgour, G., Mader, H.M., 2019a. Low analytical totals in EPMA of hydrous silicate glass due to sub-surface charging: Obtaining accurate volatiles by difference. Chem. Geol. 505, 48–56. https://doi.org/10.1016/J.CHEMGEO.2018.11.015
Hughes, E.C., Mazot, A., Kilgour, G., Asher, C., Michelini, M., Britten, K., Chardot, L., Feisel, Y., Werner, C.,

2019b. Understanding Degassing Pathways Along the 1886 Tarawera (New Zealand) Volcanic Fissure by Combining Soil and Lake CO2 Fluxes. Front. Earth Sci. 7, 264. https://doi.org/10.3389/feart.2019.00264
Jackson, M.D., Blundy, J., Sparks, R.S.J., 2018. Chemical differentiation, cold storage and remobilization of magma in the Earth's crust. Nature 564, 405–409. https://doi.org/10.1038/s41586-018-0746-2
Johnson, E.R., Kamenetsky, V.S., McPhie, J., Wallace, P.J., 2011. Degassing of the H2O-rich rhyolites of the Okataina Volcanic Center, Taupo Volcanic Zone, New Zealand. Geology 39, 311–314. https://doi.org/10.1130/G31543.1
Kay, S.M., Coira, B.L., Caffe, P.J., Chen, C.H., 2010. Regional chemical diversity, crustal and mantle sources and evolution of central Andean Puna plateau ignimbrites. J. Volcanol. Geotherm. Res. 198, 81–111. https://doi.org/10.1016/J.JVOLGEORES.2010.08.013
Keam, R.F., 1988. Tarawera: The volcanic eruption of 10 June 1886 A.D. Published by the author, Auckland.
Kilgour, G., Blundy, J., Cashman, K., Mader, H.M., 2013. Small volume andesite magmas and melt-mush interactions at Ruapehu, New Zealand: Evidence from melt inclusions. Contrib. to Mineral. Petrol. 166, 371–392. https://doi.org/10.1007/S00410-013-0880-7/FIGURES/11
Kilgour, G., Moune, S., Christenson, B., Pasqua, F. Della, 2021. Insights into the 1976–2000 eruption episode of Whakaari/White Island, New Zealand: an eruption fuelled by repeated mafic recharge. Bull. Volcanol. 83, 1–21. https://doi.org/10.1007/S00445-021-01460-5/FIGURES/12
Kress, V.C., Carmichael, I.S.E., 1991. The compressibility of silicate liquids containing Fe2O3 and the effect of composition, temperature, oxygen fugacity and pressure on their redox states. Contrib. to Mineral. Petrol. 108, 82–92. https://doi.org/10.1007/BF00307328
Law, S., Bromiley, G.D., Kilgour, G.N., Fitton, J.G., 2021. Tracing mantle source variation through xenocrystic olivine in the Taupo Volcanic Zone, New Zealand: A role for lithospheric mantle in the shift from andesitic to rhyolitic compositions. Lithos 394–395, 106185. https://doi.org/10.1016/J.LITHOS.2021.106185
Law, S., Kilgour, G., Bromiley, G.D., Boyce, A.J., n.d. Along arc variation in monogenetic mafic magmas from the Taupo Volcanic Zone, New Zealand: Insights from the crystal cargo and oxygen isotopes. J. Petrol.
Leonard, G.S., Cole, J.W., Nairn, I.A., Self, S., 2002. Basalt triggering of the c. AD 1305 Kaharoa rhyolite eruption, Tarawera Volcanic Complex, New Zealand. J. Volcanol. Geotherm. Res. 115, 461–486. https://doi.org/10.1016/S0377-0273(01)00326-2
Lloyd, A.S., Plank, T., Ruprecht, P., Hauri, E.H., Rose, W., 2013. Volatile loss from melt inclusions in pyroclasts of differing sizes. Contrib. to Mineral. Petrol. 165, 129–153. https://doi.org/10.1007/s00410-012-0800-2
Lowenstern, J.B., 2003. Melt inclusions come of age: Volatiles, volcanoes, and Sorby's legacy. Dev. Volcanol. 5, 1–21. https://doi.org/10.1016/S1871-644X(03)80021-9
Lowenstern, J.B., 1995. Applications of silicate-melt inclusions to the study of magmatic volatiles, in: Thompson, J.F.. (Ed.), Magmas, Fluids and Ore Deposits. Mineralogical Assoication of Canada Short Course Volume No.23. pp. 71–99.
Maclennan, J., 2017. Bubble formation and decrepitation control the CO2 content of olivine-hosted melt inclusions. Geochemistry, Geophys. Geosystems 18, 597–616. https://doi.org/10.1002/2016GC006633
Marxer, F., Ulmer, · Peter, Müntener, · Othmar, 2021. Polybaric fractional crystallisation of arc magmas: an experimental study simulating trans-crustal magmatic systems. Contrib. to Mineral. Petrol. 2021 1771 177, 1–36. https://doi.org/10.1007/S00410-021-01856-8
Mazot, A., Schwandner, F.M., Christenson, B., de Ronde, C.E.J., Inguaggiato, S., Scott, B.J., Graham, D., Britten, K., Keeman, J., Tan, K., 2014. CO2 discharge from the bottom of volcanic Lake Rotomahana, New Zealand. Geochemistry, Geophys. Geosystems 15, 577–588. https://doi.org/10.1002/2013GC004945
Moore, L.R., Gazel, E., Tuohy, R., Lloyd, A.S., Esposito, R., Steele-MacInnis, M., Hauri, E.H., Wallace, P.J., Plank, T., Bodnar, R.J., 2015. Bubbles matter: An assessment of the contribution of vapor bubbles to melt inclusion volatile budgets. Am. Mineral. 100, 806–823. https://doi.org/10.2138/am-2015-5036
Moretti, R., Métrich, N., Arienzo, I., Di Renzo, V., Aiuppa, A., Allard, P., 2018. Degassing vs. eruptive styles at Mt. Etna volcano (Sicily, Italy). Part I: Volatile stocking, gas fluxing, and the shift from low-energy to highly explosive basaltic eruptions. Chem. Geol. 482, 1–17. https://doi.org/10.1016/J.CHEMGEO.2017.09.017
Mortimer, N., Campbell, H.J., Tulloch, A.J., King, P.R., Stagpoole, V.M., Wood, R.A., Rattenbury, M.S., Sutherland, R., Adams, C.J., Collot, J., Seton, M., 2017. Zealandia: Earth's hidden Continent. GSA Today 27, 27–35. https://doi.org/10.1130/GSATG321A.1
Müntener, O., Ulmer, P., 2018. Arc crust formation and differentiation constrained by experimental petrology. Am. J. Sci. 318, 64–89. https://doi.org/10.2475/01.2018.04
Nairn, I.A., 2002. Geology of the Okataina Volcanic Centre, scale 1:50 000. Institute of Geological and Nuclear Sciences Limited.
Nairn, I.A., 1992. The Te Rere and Okareka eruptive episodes — Okataina Volcanic Centre, Taupo Volcanic

Zone, New Zealand. New Zeal. J. Geol. Geophys. 35, 93–108. https://doi.org/10.1080/00288306.1992.9514503
Nairn, I.A., 1981. Some Studies of the Geology, Volcanic History, and Geothermal Resources of the Okataina Volcanic Centre, Taupo Volcanic Zone, New Zealand. Victoria University of Wellington, Wellington.
Nairn, I.A., 1979. Rotomahana—Waimangu eruption, 1886: base surge and basalt magma. New Zeal. J. Geol. Geophys. 22, 363–378. https://doi.org/10.1080/00288306.1979.10424105
Nairn, I.A., Cole, J.W., 1981. Basalt dikes in the 1886 Tarawera Rift. New Zeal. J. Geol. Geophys. 24, 585–592. https://doi.org/10.1080/00288306.1981.10421534
Nairn, I.A., Self, S., Cole, J.W., Leonard, G.S., Scutter, C., 2001. Distribution, stratigraphy, and history of proximal deposits from the c. AD 1305 Kaharoa eruptive episode at Tarawera Volcano, New Zealand. New Zeal. J. Geol. Geophys. 44, 467–484. https://doi.org/10.1080/00288306.2001.9514950
Nairn, I.A., Shane, P.A., Cole, J.W., Leonard, G.., Self, S., Pearson, N., 2004. Rhyolite magma processes of the ~AD 1315 Kaharoa eruption episode, Tarawera volcano, New Zealand. J. Volcanol. Geotherm. Res. 131, 265–294. https://doi.org/10.1016/S0377-0273(03)00381-0
Nandedkar, R.H., Ulmer, P., Müntener, O., 2014. Fractional crystallization of primitive, hydrous arc magmas: An experimental study at 0.7 GPa. Contrib. to Mineral. Petrol. 167, 1–27. https://doi.org/10.1007/s00410-014-1015-5
Neave, D.A., Putirka, K.D., 2017. A new clinopyroxene-liquid barometer, and implications for magma storage pressures under Icelandic rift zones. Am. Mineral. 102, 777–794. https://doi.org/10.2138/am-2017-5968
Newnham, R.M., Eden, D.N., Lowe, D.J., Hendy, C.H., 2003. Rerewhakaaitu Tephra, a land–sea marker for the Last Termination in New Zealand, with implications for global climate change. Quat. Sci. Rev. 22, 289–308. https://doi.org/10.1016/S0277-3791(02)00137-3
Nielsen, R.L., Michael, P.J., Sours-Page, R., 1998. Chemical and physical indicators of compromised melt inclusions. Geochim. Cosmochim. Acta 62, 831–839. https://doi.org/10.1016/S0016-7037(98)00024-6
O'Neill, H.S.C., 2021. The thermodynamic controls on sulfide saturation in silicate melts with application to Ocean Floor Basalts., in: Moretti, R., Neuville, D.R. (Eds.), Magma Redox Geochemistry, Geophysical Monograph Series. John Wiley & Sons, Inc., pp. 177–213. https://doi.org/10.1002/9781119473206.ch10
Panjasawatwong, Y., Danyushevsky, L. V., Crawford, A.J., Harris, K.L., 1995. An experimental study of the effects of melt composition on plagioclase-melt equilibria at 5 and 10 kbar: implications for the origin of magmatic high-An plagioclase. Contrib. to Mineral. Petrol. 118, 420–432. https://doi.org/10.1007/s004100050024
Pérez, W., Freundt, A., Kutterolf, S., 2020. The basaltic plinian eruption of the ~6 ka San Antonio Tephra and formation of the Masaya caldera, Nicaragua. J. Volcanol. Geotherm. Res. 401, 106975. https://doi.org/10.1016/j.jvolgeores.2020.106975
Peti, L., Hopkins, J.L., Augustinus, P.C., 2021. Revised tephrochronology for key tephras in the 130-ka Ōrākei Basin maar core, Auckland Volcanic Field, New Zealand: implications for the timing of climatic changes. https://doi.org/10.1080/00288306.2020.1867200 64, 235–249. https://doi.org/10.1080/00288306.2020.1867200
Pittari, A., Muir, S.L., Hendy, C.H., 2016. Lake-floor sediment texture and composition of a hydrothermally-active, volcanic lake, Lake Rotomahana. J. Volcanol. Geotherm. Res. 314, 169–181. https://doi.org/10.1016/j.jvolgeores.2016.02.025
Price, R.C., Gamble, J.A., Smith, I.E.M., Stewart, R.B., Eggins, S., Wright, I.C., 2005. An integrated model for the temporal evolution of andesites and rhyolites and crustal development in New Zealand's North Island. J. Volcanol. Geotherm. Res. 140, 1–24. https://doi.org/10.1016/j.jvolgeores.2004.07.013
Pullar, W.A., Nairn, I.A., 1972. Matahi Basaltic Tephra member, Rotoiti Breccia Formation. New Zeal. J. Geol. Geophys. 15, 446–450. https://doi.org/10.1080/00288306.1972.10422342
Putirka, K.D., 2008. Thermometers and Barometers for Volcanic Systems. Rev. Mineral. Geochemistry 69, 61–120. https://doi.org/10.2138/rmg.2008.69.3
Rasmussen, D.J., Plank, T.A., Wallace, P.J., Newcombe, M.E., Lowenstern, J.B., 2020. Vapor-bubble growth in olivine-hosted melt inclusions. Am. Mineral. 105, 1898–1919. https://doi.org/10.2138/am-2020-7377
Roedder, E., 1979. Origin and significance of magmatic inclusions. Bull. Mineral. 102, 487–510.
Rooney, T.O., Deering, C.D., 2014. Conditions of melt generation beneath the Taupo Volcanic Zone: The influence of heterogeneous mantle inputs on large-volume silicic systems. Geology 42, 3–6. https://doi.org/10.1130/G34868.1
Rooyakkers, S.M., Wilson, C.J.N., Schipper, C.I., Barker, S.J., Allan, A.S.R., 2018. Textural and micro-analytical insights into mafic–felsic interactions during the Oruanui eruption, Taupo. Contrib. to Mineral. Petrol. 173, 35. https://doi.org/10.1007/s00410-018-1461-6
Rose-Koga, E.F., Bouvier, A.S., Gaetani, G.A., Wallace, P.J., Allison, C.M., Andrys, J.A., Angeles de la Torre, C.A., Barth, A., Bodnar, R.J., Bracco Gartner, A.J.J., Butters, D., Castillejo, A., Chilson-Parks, B., Choudhary, B.R., Cluzel, N., Cole, M., Cottrell, E., Daly, A., Danyushevsky, L. V., DeVitre, C.L.,

Drignon, M.J., France, L., Gaborieau, M., Garcia, M.O., Gatti, E., Genske, F.S., Hartley, M.E., Hughes, E.C., Iveson, A.A., Johnson, E.R., Jones, M., Kagoshima, T., Katzir, Y., Kawaguchi, M., Kawamoto, T., Kelley, K.A., Koornneef, J.M., Kurz, M.D., Laubier, M., Layne, G.D., Lerner, A., Lin, K.Y., Liu, P.P., Lorenzo-Merino, A., Luciani, N., Magalhães, N., Marschall, H.R., Michael, P.J., Monteleone, B.D., Moore, L.R., Moussallam, Y., Muth, M., Myers, M.L., Narváez, D.F., Navon, O., Newcombe, M.E., Nichols, A.R.L., Nielsen, R.L., Pamukcu, A., Plank, T., Rasmussen, D.J., Roberge, J., Schiavi, F., Schwartz, D., Shimizu, K., Shimizu, N., Thomas, J.B., Thompson, G.T., Tucker, J.M., Ustunisik, G., Waelkens, C., Zhang, Y., Zhou, T., 2021. Silicate melt inclusions in the new millennium: A review of recommended practices for preparation, analysis, and data presentation. Chem. Geol. 570, 120145. https://doi.org/10.1016/j.chemgeo.2021.120145

Rowe, M.C., Carey, R.J., White, J.D.L., Kilgour, G., Hughes, E., Ellis, B., Rosseel, J.-B., Segovia, A., 2021. Tarawera 1886: an integrated review of volcanological and geochemical characteristics of a complex basaltic eruption. New Zeal. J. Geol. Geophys. 64, 296–319. https://doi.org/10.1080/00288306.2021.1914118

Sable, J.E., Houghton, B.F., Wilson, C.J.N., Carey, R.J., 2009. Eruption Mechanisms during the climax of the Tarawera 1886 basaltic Plinian eruption inferred from microtextural characteristics of the deposits, in: Thordarson, T., Self, S., Larsen, G., Rowland, S.K., Hoskuldsson, A. (Eds.), Studies in Volcanology: The Legacy of John Walker. The Geological Society of London, London, pp. 129–154.

Saper, L.M., Stolper, E.M., 2020. Controlled Cooling-Rate Experiments on Olivine-Hosted Melt Inclusions: Chemical Diffusion and Quantification of Eruptive Cooling Rates on Hawaii and Mars. Geochemistry, Geophys. Geosystems 21. https://doi.org/10.1029/2019GC008772

Sas, M., Shane, P.A., Kuritani, T., Zellmer, G.F., Kent, A.J.R., Nakagawa, M., 2021. Mush, melts and metasediments: A history of rhyolites from the Okataina Volcanic Centre, New Zealand, as captured in plagioclase. J. Petrol. https://doi.org/10.1093/petrology/egab038

Schiano, P., 2003. Primitive mantle magmas recorded as silicate melt inclusions in igneous minerals. Earth-Science Rev. 63, 121–144. https://doi.org/10.1016/S0012-8252(03)00034-5

Schmitz, M.D., Smith, I.E.M., 2004. The Petrology of the Rotoiti Eruption Sequence, Taupo Volcanic Zone: an Example of Fractionation and Mixing in a Rhyolitic System. J. Petrol. 45, 2045–2066. https://doi.org/10.1093/petrology/egh047

Seropian, G., Kennedy, B.M., Walter, T.R., Ichihara, M., Jolly, A.D., 2021. A review framework of how earthquakes trigger volcanic eruptions. Nat. Commun. 12, 1–13. https://doi.org/10.1038/s41467-021-21166-8

Seward, A., Reeves, R., Alcaraz, S., 2022. Assessment of the surface heat loss from Waimangu Geothermal Valley: Comparison of terrestrial based assessment techniques with remote sensing. J. Volcanol. Geotherm. Res. 430, 107630. https://doi.org/10.1016/J.JVOLGEORES.2022.107630

Shane, P.A., Martin, S.B., Smith, V.C., Beggs, K.F., Darragh, M.B., Cole, J.W., Nairn, I.A., 2007. Multiple rhyolite magmas and basalt injection in the 17.7 ka Rerewhakaaitu eruption episode from Tarawera volcanic complex, New Zealand. J. Volcanol. Geotherm. Res. 164, 1–26. https://doi.org/10.1016/j.jvolgeores.2007.04.003

Shane, P.A., Nairn, I.A., Smith, V.C., 2005. Magma mingling in the ~50 ka Rotoiti eruption from Okataina Volcanic Centre: implications for geochemical diversity and chronology of large volume rhyolites. J. Volcanol. Geotherm. Res. 139, 295–313. https://doi.org/10.1016/j.jvolgeores.2004.08.012

Shane, P.A., Nairn, I.A., Smith, V.C., Darragh, M.B., Beggs, K.F., Cole, J.W., 2008. Silicic recharge of multiple rhyolite magmas by basaltic intrusion during the 22.6 ka Okareka Eruption Episode, New Zealand. Lithos 103, 527–549. https://doi.org/10.1016/j.lithos.2007.11.002

Sisson, T.W., Grove, T.L., 1993. Experimental investigations of the role of H2O in calc-alkaline differentiation and subduction zone magmatism. Contrib. to Mineral. Petrol. 1993 1132 113, 143–166. https://doi.org/10.1007/BF00283225

Smith, V.C., Shane, P.A., Nairn, I.A., 2004. Reactivation of a rhyolitic magma body by new rhyolitic intrusion before the 15.8 ka Rotorua eruptive episode: implications for magma storage in the Okataina Volcanic Centre, New Zealand. J. Geol. Soc. London. 161, 757–772. https://doi.org/10.1144/0016-764903-092

Sobolev, A. V., Shimizu, N., 1993. Ultra-depleted primary melt included in an olivine from the Mid-Atlantic Ridge. Nature 363, 151–154. https://doi.org/10.1038/363151a0

Storm, S., Shane, P.A., Schmitt, A.K., Lindsay, J.M., 2011. Contrasting punctuated zircon growth in two syn-erupted rhyolite magmas from Tarawera volcano: Insights to crystal diversity in magmatic systems. Earth Planet. Sci. Lett. 301, 511–520. https://doi.org/10.1016/J.EPSL.2010.11.034

Takagi, D., Sato, H., Nakagawa, M., 2005. Experimental study of a low-alkali tholeiite at 1-5 kbar: Optimal condition for the crystallization of high-An plagioclase in hydrous arc tholeiite. Contrib. to Mineral. Petrol. 149, 527–540. https://doi.org/10.1007/s00410-005-0666-7

Tattitch, B., Chelle-Michou, C., Blundy, J., Loucks, R.R., 2021. Chemical feedbacks during magma degassing

control chlorine partitioning and metal extraction in volcanic arcs. Nat. Commun. 2021 121 12, 1–11. https://doi.org/10.1038/s41467-021-21887-w
Thomas, A.P.W., 1888. Report on the Eruption of Tarawera and Rotomahana, NZ, Government Printer, Wellington, New Zealand.
Thomas, R.W., Wood, B.J., 2021. The chemical behaviour of chlorine in silicate melts. Geochim. Cosmochim. Acta 294, 28–42. https://doi.org/10.1016/J.GCA.2020.11.018
Villamor, B.P., Litchfield, N.J., Gómez-Ortiz, D., Martin-González, F., Alloway, B. V., Berryman, K.R., Clark, K.J., Ries, W.F., Howell, A., Ansell, I.A., 2022. Fault ruptures triggered by large rhyolitic eruptions at the boundary between tectonic and magmatic rift segments: The Manawahe Fault, Taupō Rift, New Zealand. J. Volcanol. Geotherm. Res. 427, 107478. https://doi.org/10.1016/J.JVOLGEORES.2022.107478
Waight, T.E., Troll, V.R., Gamble, J.A., Price, R.C., Chadwick, J.P., 2017. Hf isotope evidence for variable slab input and crustal addition in basalts and andesites of the Taupo Volcanic Zone, New Zealand. Lithos. https://doi.org/10.1016/j.lithos.2017.04.009
Walker, G.P.L., Self, S., Wilson, L., 1984. Tarawera 1886, New Zealand — A basaltic plinian fissure eruption. J. Volcanol. Geotherm. Res. 21, 61–78. https://doi.org/10.1016/0377-0273(84)90016-7
Wallace, P.J., Kamenetsky, V.S., Cervantes, P., 2015. Melt inclusion CO2 contents, pressures of olivine crystallization, and the problem of shrinkage bubbles. Am. Mineral. 100, 787–794. https://doi.org/10.2138/am-2015-5029
Wilson, C.J.N., Blake, S., Charlier, B.L.A., Sutton, A.N., 2006. The 26·5 ka Oruanui Eruption, Taupo Volcano, New Zealand: Development, Characteristics and Evacuation of a Large Rhyolitic Magma Body. J. Petrol. 47, 35–69. https://doi.org/10.1093/petrology/egi066
Wilson, C.J.N., Gravley, D.M., Leonard, G.S., Rowland, J. V., 2009. Volcanism in the central Taupo Volcanic Zone, New Zealand: tempo, styles and controls. Spec. Publ. IAVCEI 225–247. https://doi.org/10.1144/IAVCEL002.12
Wilson, C.J.N., Houghton, B.F., McWilliams, M.O., Lanphere, M.A., Weaver, S.D., Briggs, R.M., 1995. Volcanic and structural evolution of Taupo Volcanic Zone, New Zealand: a review. J. Volcanol. Geotherm. Res. 68, 1–28. https://doi.org/10.1016/0377-0273(95)00006-G
Wysoczanski, R.J., Wright, I.C., Gamble, J.A., Hauri, E.H., Luhr, J.F., Eggins, S.M., Handler, M.R., 2006. Volatile contents of Kermadec Arc–Havre Trough pillow glasses: Fingerprinting slab-derived aqueous fluids in the mantle sources of arc and back-arc lavas. J. Volcanol. Geotherm. Res. 152, 51–73. https://doi.org/10.1016/J.JVOLGEORES.2005.04.021
Yang, T.-H.J., Chambefort, I., Mazot, A., Rowe, M., Scott, B., MacDonald, N., Werner, C., Fischer, T., Ronde, C. de, n.d. Understanding caldera degassing from a detailed investigation at Lake Rotoiti, Okataina Volcanic Centre, New Zealand. J. Volcanol. Geotherm. Res.
Zellmer, G.F., Kimura, J.-I., Stirling, C.H., Lube, G., Shane, P.A., Iizuka, Y., 2020. Genesis of recent mafic magmatism in the Taupo Volcanic Zone, New Zealand: insights into the birth and death of very large volume rhyolitic systems? J. Petrol. 61, egaa027. https://doi.org/10.1093/petrology/egaa027